Lawrence Berkeley National Laboratory
Recent Work

Title
A VERSATILE APPARATUS FOR MEASURING TOTAL AND DIFFERENTIAL CROSS SECTIONS FOR ION-NEUTRAL INTERACTIONS

Permalink
https://escholarship.org/uc/item/42w7w9ps

Author
Gentry, W.R.

Publication Date
1967-07-01

eScholarship.org Powered by the California Digital Library
University of California

UCRL-17691

c.2

University of California

Ernest O. Lawrence Radiation Laboratory

A VERSATILE APPARATUS FOR MEASURING TOTAL AND DIFFERENTIAL CROSS SECTIONS FOR ION-NEUTRAL INTERACTIONS

W. R. Gentry

July 1967

RECEIVED
LAWRENCE
RADIATION LABORATORY
NOV 22 1967
LIBRARY AND
DOCUMENTS SECTI

TWO-WEEK LOAN COPY

This is a Library Circulating Copy
which may be borrowed for two weeks.
For a personal retention copy, call
Tech. Info. Division, Ext. 5545

UCRL-17691
Cy. 2

DISCLAIMER

This document was prepared as an account of work sponsored by the United States Government. While this document is believed to contain correct information, neither the United States Government nor any agency thereof, nor the Regents of the University of California, nor any of their employees, makes any warranty, express or implied, or assumes any legal responsibility for the accuracy, completeness, or usefulness of any information, apparatus, product, or process disclosed, or represents that its use would not infringe privately owned rights. Reference herein to any specific commercial product, process, or service by its trade name, trademark, manufacturer, or otherwise, does not necessarily constitute or imply its endorsement, recommendation, or favoring by the United States Government or any agency thereof, or the Regents of the University of California. The views and opinions of authors expressed herein do not necessarily state or reflect those of the United States Government or any agency thereof or the Regents of the University of California.

UCRL-17691
UC-37 Instruments
TID-4500 (50th Ed.)

UNIVERSITY OF CALIFORNIA
Lawrence Radiation Laboratory
Berkeley, California

AEC Contract No. W-7405-eng-48

A VERSATILE APPARATUS FOR MEASURING TOTAL AND DIFFERENTIAL CROSS SECTIONS FOR ION-NEUTRAL INTERACTIONS

W. R. Gentry

July 1967

Printed in the United States of America
Available from
Clearinghouse for Federal Scientific and Technical Information
National Bureau of Standards, U.S. Department of Commerce
Springfield, Virginia 22151
Price: Printed Copy $3.00; Microfiche $0.65

Table of Contents

List of Illustrations..... v

Acknowledgments..... vii

Introduction..... 1

Chapter I

Discussion of Design Criteria..... 4

Resolution..... 7

Background Signal and Pumping Speed..... 7

Ion Beam..... 9

Neutral Beam 10

Considerations of Detector Sensitivity..... 11

Chapter II

General Description 17

Chapter III

Detailed Descriptions of Components 23

A. Main Chamber 23

B. Ion Beam Sources, Focusing System, and Monitors..... 27

1. Electron Bombardment Source..... 27

2. Alkali Metal Ion Source 31

3. Ion Beam Analysis and Focusing System..... 34

Design Features 38

Operation 41

4. Ion Beam Monitors 42

C. Neutral Gas Targets and Monitors 42

1. Collision Cell 42

2. Nozzle Source for Alkali Metal Beams 44

3. Multichannel Beam Source 47

4. Nozzle Beam Source for Permanent Gases..... 49

5. Neutral Beam Monitors and Detectors 49

D. Product Ion Analysis System..... 51

1. Spherical Electrostatic Energy Analyzer 52

2. First Detection System Focusing Stage 55

3. Quadrupole Mass Spectrometer 56

4. Second Detection System Focusing Stage 56

E. Ion Counter 56

1. General 56

2. Construction 59

3. Instrumentation 60

4. Operation 61

5. Resolution and Efficiency 63

6. Stability 67

Chapter IV

Operation and Data Analysis 68

A. Measurement of the Total Absolute Resonant Charge Transfer Cross Sections for Cs^+-Cs, Rb^+-Rb, and K^+-K in the 10 - 500eV Energy Range 68

1. Experimental Arrangement and Instrumentation 69

2. Procedure 71

General 71

Attenuation Method 72

Slow Ion Collection Method 74

Measurement of the Neutral Beam Distribution..... 74

3. Calculation of the Cross Section 75

4. Discussion of Errors 81

Average Velocity 81

Diatomic Molecules in the Neutral Beam 81

Ionization Coefficient 82

Contribution to the Scattering Fraction by Processes other than Charge Transfer 82

B. Collision Cell Measurements of Product Energy and Angular Distributions from Ion-Molecule Reactions 84

1. General 84

2. Experimental Arrangement and Instrumentation 85

3. Procedure 88

4. Data Analysis 90

References 96

Bibliography 98

Appendix A

List of Currently Available Mechanical Drawings 100

A. Molecular Beam Reaction Chamber 100

B. Ion Beam Source (Alkali Metal) 100

C. Ion Beam Focusing System 101

D. Molecular Beam Source (Alkali Metal) 101

E. Permanent Gas Multichannel Beam Source 102

F. Supersonic Nozzle Beam 102

G. Ion Scattering Cell 103

H. Molecular Beam Detector (Alkali Metal) 103

I. Molecular Beam Detector (Permanent Gas) 103

J. Ion Beam Detector (with Retarding Electrode) 104

K. Ion Detector (with QPMS and MEM) 104

L. Ion Counter 104

M. Fixed Faraday Cup Detector 105

N. Spherical Energy Analyzer 105

Appendix B

List of Electronic Prints 106

A. Vacuum System 106

B. Experimental Instrumentation 106

List of Illustrations

Fig. 1 Schematic diagram of a typical crossed beam experiment.... 6

Fig. 2 Schematic diagrams of three types of neutral beam source.. 11

Fig. 3 View of the apparatus 18

Fig. 4 View of the apparatus 19

Fig. 5 View of the apparatus 20

Fig. 6 Main Chamber. Inset shows detail of tec-ring seal..... 24

Fig. 7 Electron impact ion source 28

Fig. 8 Photograph of electron bombardment ion source 29

Fig. 9 Thermal ionization source for alkali metal ions 32

Fig. 10 Ion beam focusing and analysis system schematic (horizontal section) shown with electron bombardment ion source 36

Fig. 11 Ion beam focusing and analysis system (horizontal section) Block diagram of power supply connections 37

Fig. 12 Ion beam analysis magnet 40

Fig. 13 Collision cell..... 43

Fig. 14 Alkali metal nozzle beam source 45

Fig. 15 Multichannel beam source 48

Fig. 16 Schematic diagram of crossed beam experiment with multi-channel beam source 50

Fig. 17 Vertical section of product ion detection system 53

Fig. 18 Cutaway drawing of ion counter 58

Fig. 19 Detector pulse height distribution for 25 keV N_2^+ ions, showing resolved peaks corresponding to integer numbers of electrons in the emission pulse 65

Fig. 20 Schematic diagram of the apparatus set up for measurement of alkali metal charge transfer cross sections 70

Fig. 21 Alkali metal neutral beam detector geometry 77

Fig. 22 Schematic diagram of the apparatus set up for collision cell measurements of product ion energy and angular distributions 86

Fig. 23 Photograph of the main chamber interior, showing ion lens focusing element shield, collision cell, and detector set at $\theta = 0^\circ$ 87

ACKNOWLEDGMENTS

It is a pleasure to acknowledge here the very numerous and important contributions made by Dr. Yuan-tseh Lee, whose capacity for rapidly absorbing the technology necessary to do a given job is exceeded only by the rate at which he gets the job done. Dr. Lee was responsible jointly with the author for the design, construction and early operation of the apparatus, and deserves to share at least equally in whatever expletives future inheritors of the instrument will direct toward its originators in moments of jubilation or despair.

The valuable ideas contributed by Dr. Bruce H. Mahan, who originally conceived the project, are likewise gratefully acknowledged. In addition to his contributions of a scientific or technological nature, Dr. Mahan displayed in remarkable abundance that quality of penultimate importance in research directors--the ability to locate the financial resources to see his students through periods of fiscal emergency brought on by their insufficient planning.

Among the many contributions made to the apparatus design by members of the Lawrence Radiation Laboratory mechanical and electronic engineering staffs, those of Mr. Gerd Behrsing, who aided in much of the early mechanical design, and of Mr. Donald Landis, who helped adapt the semiconductor radiation detector to the counting of slow ions, are especially worthy of mention.

Many of the operating procedures have been semi-finalized in experiments run with the aid of Dr. Eric A. Gislason and Mr. Chi-wing Tsao. Mr. Tsao also participated in some of the later design work. The author is also grateful to Dr. Gislason for valuable discussions on the data

analysis, for writing the computer programs, and for proofreading this manuscript, to which he has made numerous significant contributions.

Finally, the author wishes to acknowledge three years of support through a Graduate Fellowship from the National Science Foundation.

This work was performed under the auspices of the United States Atomic Energy Commission.

INTRODUCTION

Ever since chemists began describing chemical reactions in terms of elementary dynamic processes, the evolution of the experimental techniques of chemical kinetics has naturally been motivated by the desire to isolate these elementary processes and to study them individually. For monomolecular events this isolation is relatively very simple, as demonstrated by the early and rapid development of spectroscopy. In order to isolate an elementary bimolecular process, however, one must first insure that the property of the system one is investigating be due strictly to single interactions (generically termed "collisions") between the two molecules.

The intersection of two beams of molecules under high vacuum conditions provides an elegantly direct method for studying single bimolecular collisions.* More importantly, this method allows one a means of controlling - to the limits of his technological capability - the initial conditions of the process he is studying--such as the direction of approach of the two molecules, their relative velocity, and even their electronic and rotational states.[3,4] Furthermore, many details of the collision dynamics can be deduced directly from the final velocity vector and state distributions of the products, which are, in principle, measurable in such an experiment.

This report describes a beam apparatus for studying the dynamics of ion-neutral interactions in the primary ion energy range 5-500 eV. The apparatus was designed and constructed jointly with Dr. Yuan-tseh Lee,

---

* A complete bibilography for molecular beam studies of chemical reactions has been given by Herschbach.[1] For more recent reviews covering other applications of the beam technique see Ross.[2]

under the direction of Professor Bruce H. Mahan, and was fabricated in the shops of the Lawrence Radiation Laboratory and Chemistry Department of the University of California, Berkeley. Except for some preliminary work on the electron bombardment ion beam source, the design work was begun in June, 1965. The apparatus was designed primarily with the study of chemical reactions in mind, although great care was taken to achieve as much versatility as practical in the interchangability of components, to allow a wide variety of ion-neutral processes to be studied without irreversible modifications to the equipment.

At the time construction was begun, no measurements of energy and angular distributions of products from ion-molecule collisions had been reported. As of this publication date there have been three such studies known to the author, done by Champion, Doverspike and Bailey,[5,6] at the University of Florida, and by Herman, et al.,[7] at Yale University, in addition to those done at this laboratory. There has also been one crossed beam study made of an ion-molecule reaction where only the angular distribution was measured.[8]

The experiments done so far with our instrument are the following:

1. Measurements of the absolute total resonant charge-transfer cross sections for Cs^+-Cs, Rb^+-Rb and K^+-K, in the 10-500 eV energy range.[9*]

2. Determination of the energy and angular distributions of all isotopic products from the reactions

$$N_2^+ + H_2,\ D_2,\ HD \longrightarrow N_2H^+,\ N_2D^+ + H,D$$

in the energy range 25-135 eV.[10]

---

* Abstracts of work given in the 1966 Annual Report of the Inorganic Materials Research Division of the Lawrence Radiation Laboratory (UCRL-17330).

3. Measurements of energy and angular distributions of N_2H^+ from $N_2^+ + CH_4$ collisions from 10 eV to 75 eV.*†

4. Measurements of energy and angular distributions of N_2D^+ from $N_2^+ + C_2D_2$ collisions at energies between 25 and 65 eV.†

5. Determination of inelasticity as a function of scattering angle for N_2^+ collisions with He.[11]

6. Observation of inelastic collisions giving large angle scattering of N_2^+ from D_2.†

A crossed beam method was used in the first study. The subsequent experiments were performed by passing the ion beam through a scattering cell containing the target gas.

This report will discuss first the criteria considered in the design of the apparatus, then go on to the description of the individual components and their interrelation. It will conclude with discussions of the experimental operation and the analysis of the data. In the last section, the two modes of operation by which data have already been obtained will be used to illustrate what may be done with the equipment. Happily, these two modes cover both the measurement of total and differential cross-sections, crossed beam and scattering cell techniques, and the operation of both the alkali metal and the permanent gas beam sources and detectors. Future additions and improvements to the equipment which have been planned will be mentioned where appropriate.

---

* Abstracts of work given in the 1966 Annual Report of the Inorganic Materials Research Division of the Lawrence Radiation Laboratory (UCRL-17330).

† Unpublished results.

CHAPTER I

Discussion of Design Criteria

Most of the difficulties involved in doing beam experiments are directly tied to the product intensity obtainable under the required experimental conditions. A statistic customarily cited by experimenters in this field in order to impress non-specialists with the sensitivity of their equipment is the time required to deposit a monolayer of product molecules on the detector. With one of the first alkali metal crossed beam instruments, where a surface ionization detector was used, this figure was as high as one month for some of the measured intensities.[12] With later modifications for beam modulation, product mass selection and detection with an electron multiplier, the monolayer deposition time went up to 100 years.[13] In our experiments, product ion fluxes at the ion counter of less than one ion/cm^2-sec were readily measured. At this rate the time required for deposition of a monolayer is approximately 100,000,000 years.

The cross section for the process of interest and the types of primary beam sources used obviously limit the intensity of product ions one can obtain. Unfortunately, an experiment cannot be designed around these factors alone; there are many other parameters which affect the usable sensitivity of the apparatus.

A primary requirement for beam experiments is a vacuum sufficiently good that all (or at least a measureable fraction) of the signal one observes originates from single collisions of the reactants in the intersection volume. In general, this means that not only must the background pressure not significantly attenuate the primary or secondary beams, but

that the intensities of products from collisions with background molecules be either small relative to the signal or in some way subtractable. Thus, the intensity one can use in a neutral beam is often limited not only by the type of source used but also by the pumping speed of the vacuum system for the beam gas and the background signal requirements for the reaction being studied.

Similarly, the ion beam intensity is determined not only by the rate at which the source can generate ions, but also by the experimental energy and mass resolution requirements, and by the space-charge spreading of the ion beam profile due to mutual Coulomb repulsion of the ions.

The detection sensitivity necessary to do a given experiment depends, in turn, on the reactant beam intensities obtainable under the above limitations, the total cross section for the process being investigated, and additionally on the product mass, energy and angular resolution required and on the dynamics of the reaction itself. Of course, any additional state selection, such as velocity selection of the neutral beam or electronic or rotational state selection of the reactants or products, will result in decreased intensity.

To illustrate these problems, let us consider the experimental arrangement shown schematically in Fig. 1. This approximates one of the modes in which our apparatus may be operated. Here, a velocity selected ion beam is crossed at right angles with a differentially pumped neutral beam. Products emerging at an angle θ with respect to the ion beam are energy selected and detected. For simplicity, the beams are assumed to be perfectly collimated, and mass selection is ignored. The residual pressure in the chamber not due to the neutral beam is assumed negligible.

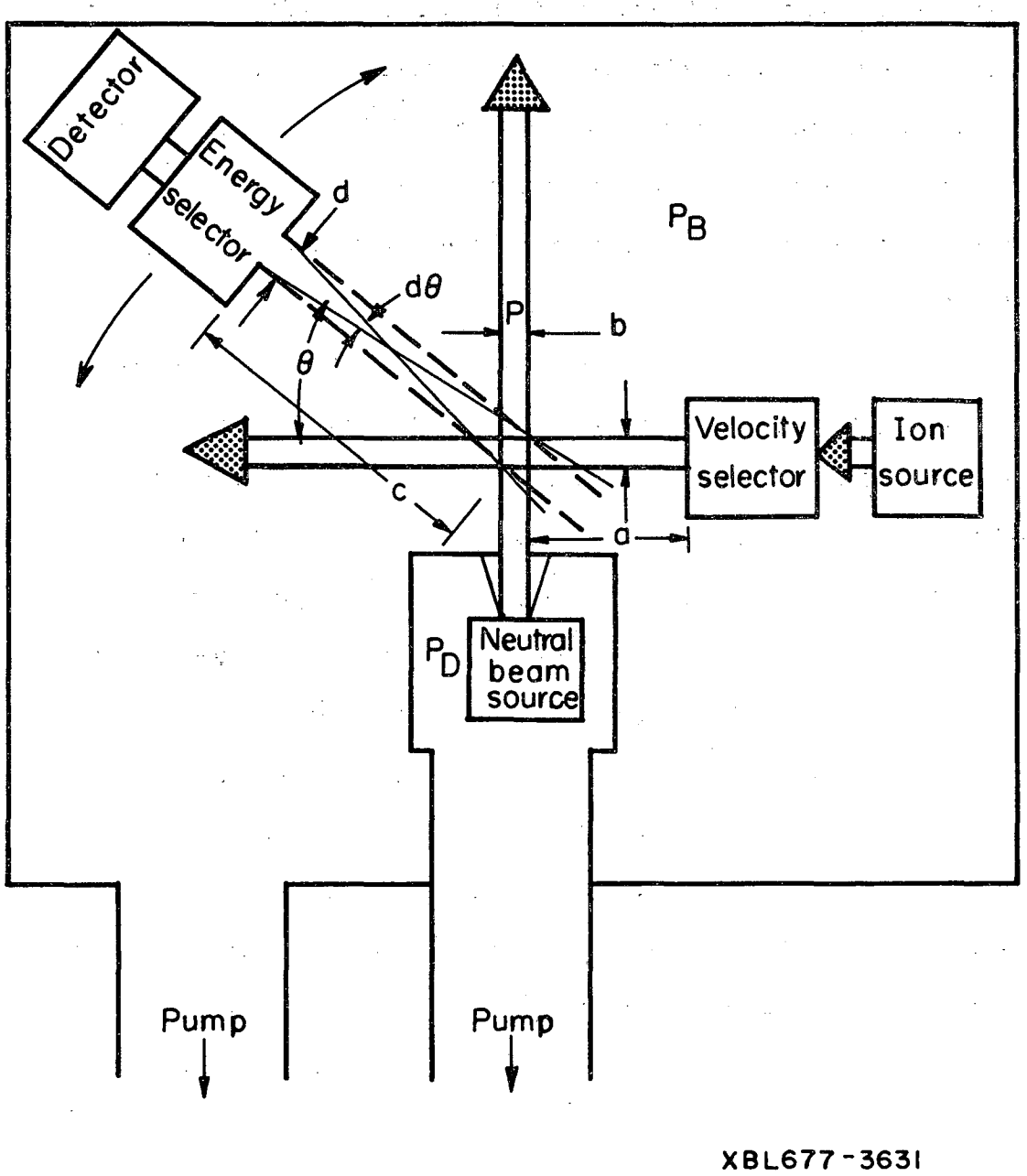

Fig. 1. Schematic diagram of a typical crossed beam experiment

Resolution

A few observations may be made immediately. The detector resolution full-width $d\theta$ is seen to be determined by the widths of the beams and of the detector aperture, and the distance between the detector aperture and the crossing point. In order to simplify analysis of the data, it is desirable that this resolution not change with the detector angle θ; hence the beams should be of approximately the same width at the crossing point. Also, since the beam intensities available are, in general, roughly proportional to the allowable widths of the beams, the optimum compromise between product intensity and detector angular resolution is obtained when the detector aperture diameter is approximately equal to the beam widths.

Background Signal and Pumping Speed

If product ions having the correct energy and angle can only originate in collisions between the ions in the primary beam and molecules of the neutral beam gas, then the ratio of the true signal I to the background signal I_B will be approximately

$$\frac{I}{I_B} = \frac{P}{P_B} \frac{V_I}{V_D} \qquad (1)$$

where P and P_B are respectively the pressure of the neutral beam gas in the beam at the crossing point and in the background, and where V_I and V_D are respectively the volumes of the ion beam intersected by the neutral beam and by the detector aperture projection (dashed lines). The worst case is for $\theta = 0°$. The ratio is then

$$\left(\frac{I}{I_B}\right)_{0°} = \frac{P}{P_B} \frac{b}{a+c} \qquad (2)$$

where a, b, and c are the dimensions shown.

In order for $d\theta$ to be small, it is necessary to have $c \gg b$, making it a requirement that $P \gg P_B$ just for the signal to be equal to the background. The pressures are related by the steady-state flow equation for the system. If the neutral beam profile at the crossing point has an area A, the collimating slit an area A', and if the average velocity of the particles is $\bar{v}_b$ in the beam and $\bar{v}_d$ in the differential pumping chamber, then the condition for steady state flow is

$$P_B C = PA\bar{v}_b + \frac{P_D A' \bar{v}_d}{4} \qquad (3)$$

where C is the volume pumping speed of the vacuum system. The second term on the right-hand side of Eq. (3) comes from molecular flow of the neutral beam gas from the differential pumping chamber through the collimating slit. If the differential pumping is efficient enough to make this term negligible, then

$$\frac{P}{P_B} = \frac{C}{A\bar{v}_b} \qquad (4)$$

For example, if C = 1000 liters/sec, A = 0.2 cm^2 and $\bar{v}_b = 5 \times 10^4$ cm/sec, then one would expect $P/P_B = 100$ if all the background gas comes from the neutral beam. Under these conditions, if one requires a detector angular resolution $d\theta = 1^\circ$, then by Eq. (2) the background signal will be at least as large as the true signal at small θ. The only way to improve the signal to background ratio in the apparatus as shown in Fig. 1 is to increase the pumping speed C. If the beam gas is condensable, it may be trapped with an effectively infinite pumping speed, which reduces the background problem enormously. It is also possible to differentially pump the neutral beam after it intersects the ion beam. This will be

discussed later.

Ion Beam

The space-charge broadening of an initially collimated ion beam of circular cross section is given approximately by[14]

$$\frac{X}{\ell} = \left[4.1 \times 10^{6} \frac{\sqrt{M}\, j}{E_i^{o\,3/2}} \right]^{1/2} \text{cm}^{-1} \qquad (5)$$

for

$$2 < X < 5$$

where the broadening is expressed as the fraction X of the initial beam width per unit distance l in cm. The ion mass to charge ratio M is in a.u. per electron charge, the current density j in amp/cm^2, and the ion energy E_i^o in eV. For example, if a broadening of the ion beam width of a factor of 2 per 40 cm is acceptable, then the maximum current density which can be used is

$$j = 6.1 \times 10^{-10} \frac{E_i^{o\,3/2}}{\sqrt{M}} \text{ amp/cm}^2. \qquad (6)$$

For a typical beam of 10 eV N_2^+ ions having an initial cross section of 0.1 cm^2, the current is limited by this criterion to only 3.6×10^{-10} amp.

The ion beam intensity is further restricted by the velocity resolution required in the final beam. If the primary beam velocity spread required for a given experiment is dv^o and the velocity spread of ions emitted by the source is dv_s, then the ratio of ion current in the final beam to that emitted by the source is (to first order)

$$\frac{i^o}{i_s} \leq \frac{dv^o}{dv_s} \qquad (7)$$

where the equality holds only if the focusing is perfect. Since space-charge defocusing of the beam will always decrease the current ratio in Eq. (7), regardless of the initial quality of the focusing system design, the optimum operating conditions for the ion source will be a compromise between the ion current emitted and the space-charge defocusing. It is clear that in the design of the focusing and analysis sytems that the ion path should be kept as short as possible in regions where the combination of small beam profile and low energy give spreading which is large by Eq. (5).

Neutral Beam

Three general types of sources yielding neutral beams in the thermal energy range have been successfully used in crossed beam experiments. These have been compared by Anderson, Andres and Fenn.[15] In order of increasing efficiency (and increasing complexity) they are the simple effusion source, the multichannel source, and the nozzle source. The features pertinent to the design of the apparatus are summarized below:

a. The simple effusion source, shown in Fig. 2a, depends for its operation purely on random molecular flow through the slit in the beam "oven". It operates most efficiently when the mean free path of the molecules at pressure P_1 is greater than the diameter of the source slit. Under these conditions the angular distribution of intensity is given by

$$I(\alpha) = \frac{n\bar{v}_a}{4\pi} \frac{A_s}{\ell^2} \cos\alpha \qquad (8)$$

where n is the number density of molecules in the source, $\bar{v}_a$ is the average velocity of particles in the oven, ℓ is the radial distance from the slit, and A_s is the area of the slit. Only that fraction of the

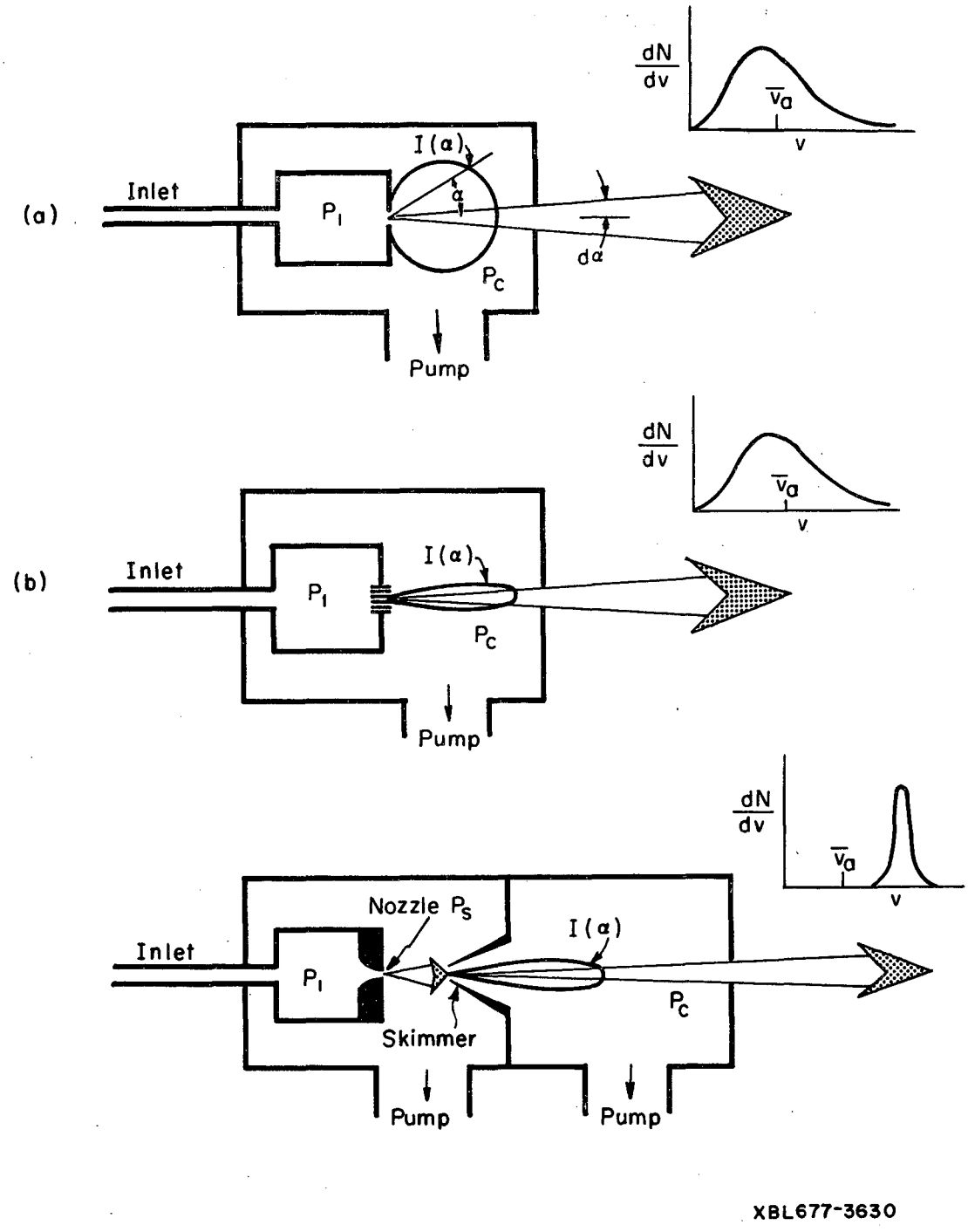

Fig. 2. Schematic diagrams of three types of neutral beam source (a) Simple effusion source; (b) Multichannel slit source; (c) Nozzle source. $\bar{v}_a$ is the Maxwellian average velocity of the molecules in the source chamber at P_1.

intensity which is within $d\alpha$ of the beam centerline will contribute to the beam intensity; the rest must be pumped out in the differential pumping stage. The centerline velocity distribution is Maxwellian.

b. The slit of the multichannel source in Fig. 2b consists of a parallel array of tiny channels having lengths large compared to their diameters. For optimum efficiency the source pressure is adjusted such that the mean free path of the molecules at pressure P_1 is greater than the channel length. Under these conditions only those molecules having velocity vectors with $\alpha \sim 0^\circ$ will pass unhindered through the slit. This results in an intensity distribution $I(\theta)$ as shown, where a much larger fraction of the total gas flow contributes to the usable beam intensity than in the case of the simple effusion source. The centerline velocity distribution for the multichannel source is Maxwellian under ideal conditions, but may differ slightly from a Maxwellian distribution if P_1 is made too high.[16]

c. The nozzle beam source shown in Fig. 2c is operated at relatively very high pressures P_1, such that the mean free path of the molecules is much less than the minimum nozzle diameter. In this way, mass flow through the converging section of the nozzle is obtained, followed by free expansion into the skimmer chamber at pressure $P_s \ll P_1$. The skimmer serves to partially collimate the beam and is shaped so as to cause the shock wave through the expanding gas to be attached to the apex of the skimmer, rather than to be ahead of the skimmer where it would cause attenuation of the beam. A second slit serves to collimate the final beam. Mass flow through the nozzle gives the molecules a directed velocity along the beam centerline which, under conditions of high compression, is large relative to their random thermal velocities.

Since the expansion after passing through the nozzle is adiabatic, the temperature of most gases is markedly decreased in the expansion process. The combination of these effects gives a velocity distribution of small width relative to a Maxwellian distribution, and shifted to higher velocities. Although the total gas flow through the nozzle beam source is much greater than that through either of the other sources, the bulk of the differential pumping is done in the skimmer chamber, making the nozzle beam source more efficient than the multichannel source for a given beam divergence and collimating chamber pumping speed.

A rule-of-thumb for the relative intensities obtainable with these sources for a given pumping speed limitation is that a well-designed multichannel ource will give an intensity somewhat more than a factor of ten greater than that of a simple effusion source, and that a nozzle beam source will give an intensity about a factor of ten greater than that of a multichannel source. The nozzle beam source is clearly superior to the multichannel source in both intensity and velocity resolution; however, it does have the disadvantage that it is much more difficult to construct and operate. There are also problems with nucleation and condensation in the beam with gases which are condensable at the final beam temperature and pressure in the skimmer.[17] Another drawback is that the velocity distribution from the nozzle source cannot be calculated and hence must be determined experimentally for each gas used. Finally, the amount of gas consumed by a nozzle beam source (typically several liters per hour for a source scaled to our apparatus dimensions) almost precludes its use with rare isotopes.

Considerations of Detector Sensitivity

A simple and direct method for measuring absolute ion currents is to allow the ions to impinge on a metal surface connected to an electrometer. The probability of an ion's losing its charge upon collision with a metal is virtually unity provided the ionization potential is greater than the surface work function; and at the energies of interest here the emission of secondary electrons by ion impact is small. With a good vibrating reed electrometer, currents down to the region of 10^{-15} amp, or 10^{4} ions/sec may be measured without undue difficulty. The next step in extending the sensitivity is to precede the electrometer with a multistage electron multiplier. By this means currents of the order of 1 ion/sec may be measured, although problems are introduced by the fact that the gain of most electron multipliers changes with time and is not the same for different ions. Clearly, the ultimate sensitivity is obtained if each ion striking the detector is magnified into a current pulse, and the pulses counted. Provided the background counting rate is low, the only limitation to the intensities one can measure by this method is the length of time one is willing to take for each measurement. Also, if all the pulses are counted regardless of their magnitude, the exact gain of the multiplier is unimportant in measuring absolute intensities.

The total product ion intensity in a particular crossed beam experiment is determined solely by the intensities and dimensions of the two beams and the cross section for the process giving that product. The detector sensitivity necessary to do a given experiment depends additionally, however, on the dynamics of the process itself and on the mass ratios of reactants and products. If g_{ion} is the final center

of mass (CM) velocity of the charged product of the reaction of a primary ion with energy E_i^o moving in a path perpendicular to the path of a neutral molecule having energy E_n^o, then the largest laboratory angle relative to that of the center of mass velocity vector at which this product can be found is given by

$$\tan \theta_{max} = \frac{g_{ion}}{v_{cm}} \quad . \tag{9}$$

From straightforward conservation of energy and momentum relations, the velocity ratio g_{ion}/v_{cm} can be expressed in terms of the masses of the reactants and products by

$$\left(\frac{g_{ion}}{v_{cm}}\right)^2 = \frac{m_f}{M_f} \frac{(M_t Q + m_i E_i^o + M_i E_n^o)}{(M_i E_i^o + m_i E_n^o + 2\sqrt{M_i E_i^o}\sqrt{m_i E_n^o})} \tag{10}$$

where M_i = initial ion mass

m_i = initial neutral mass

M_f = final ion mass

m_f = final neutral mass

M_t = total mass = $M_i + m_i = M_f + m_f$

Q = exothermicity of the reaction.

The average neutral beam energy for the simple effusion and multi-channel sources is about 10^{-4} T (eV), where T is the oven temperature in °K. For the nozzle beam source, the average beam energy is only a factor of 2 or 3 higher than this. Therefore for the ion energies of interest here, $E_i^o \gg E_n^o$. It can be seen then from Eq. (10) that unless the reaction is extremely exothermic the conditions that <u>both</u> $M_i \gg m_i$

and $M_f \gg m_f$ are sufficient to confine all the products to a very small region of laboratory angle, making detection relatively easy, but at a cost of angular resolution in the cm coordinate system.

CHAPTER II

General Description

The general layout of the equipment can be seen from the photographs in Figs. 3-5, which show the apparatus with the electron bombardment ion source, the target gas scattering cell and the ion counter detection system mounted. Many of the cables have been removed in Figs. 4 and 5 to avoid unnecessary complication of the photographs.

The collision region is in the center of the main vacuum chamber A, which has the internal dimensions 21"×21"(width) ×11"(height). This chamber has a large port in the center of each vertical side in which ion and neutral beam source components and monitors are mounted. The product ion and other detectors are mounted on a 20" diameter section B of the top of this chamber, which is capable of rotating under high vacuum. This lid is graduated around its circumference in degrees. A vernier reading in minutes is inscribed on a ring attached to the chamber to allow precise setting of the detector angle. An additional port in the center of the lid can be used to mount a scattering cell or other component, such as a neutral beam source (for measurements of out-of-plane scattering) or a photomultiplier tube (for studies of collision-induced radiation or chemiluminescence). The lid is rotated manually by a chain and sprocket drive.

Pumping for the main chamber is provided by two six-inch oil diffusion pumps, one mounted below the center of the chamber and the other mounted beneath the tee C where it can provide differential pumping for a neutral beam source. These pumps are equipped with liquid nitrogen cooled baffles, and hold the chamber at a residual pressure of

Figs. 3-5 Three views of the apparatus. The following index refers to all three figures.

A Main chamber

B Rotating lid

C Main chamber tee

D Tube for differential pumping of tec-ring seal

E Support frame

F Ion source

G Ion source vacuum chamber

H Mass spectrometer chamber

I Momentum analysis magnet

J Support flange for ion beam final focusing stage

K Teletypewriter and tape punch

L X-Y recorder

M Mounting flange for liquid nitrogen reservoir

N Leak valves for target gas

O Leak valve for ion beam gas

P Quadrupole mass filter chamber

Q FET preamplifier

R Detector liquid nitrogen reservoir

S Ion beam monitor flange

T Drive sprocket for rotating lid

U Stationary arm for holding collision cell inner cylinder fixed

V Collision cell ion gauge tube

W Liquid nitrogen manifold and solenoid valve for filling diffusion pump baffles

X Ion beam gas reservoir

Y Target gas reservoir

Z Flange for mounting multi-channel slit beam source controls

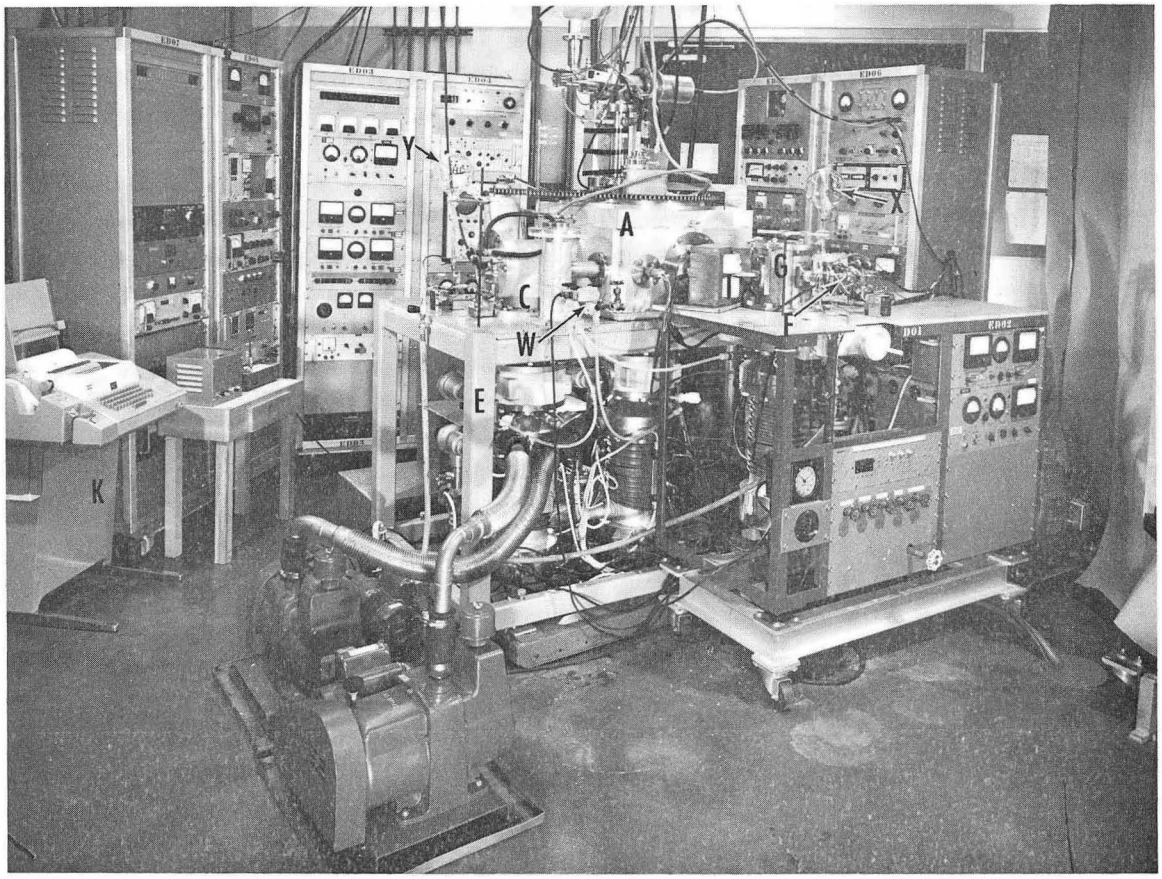

XBB 670-5734

Fig. 3.

XBB 670-5731

Fig. 4.

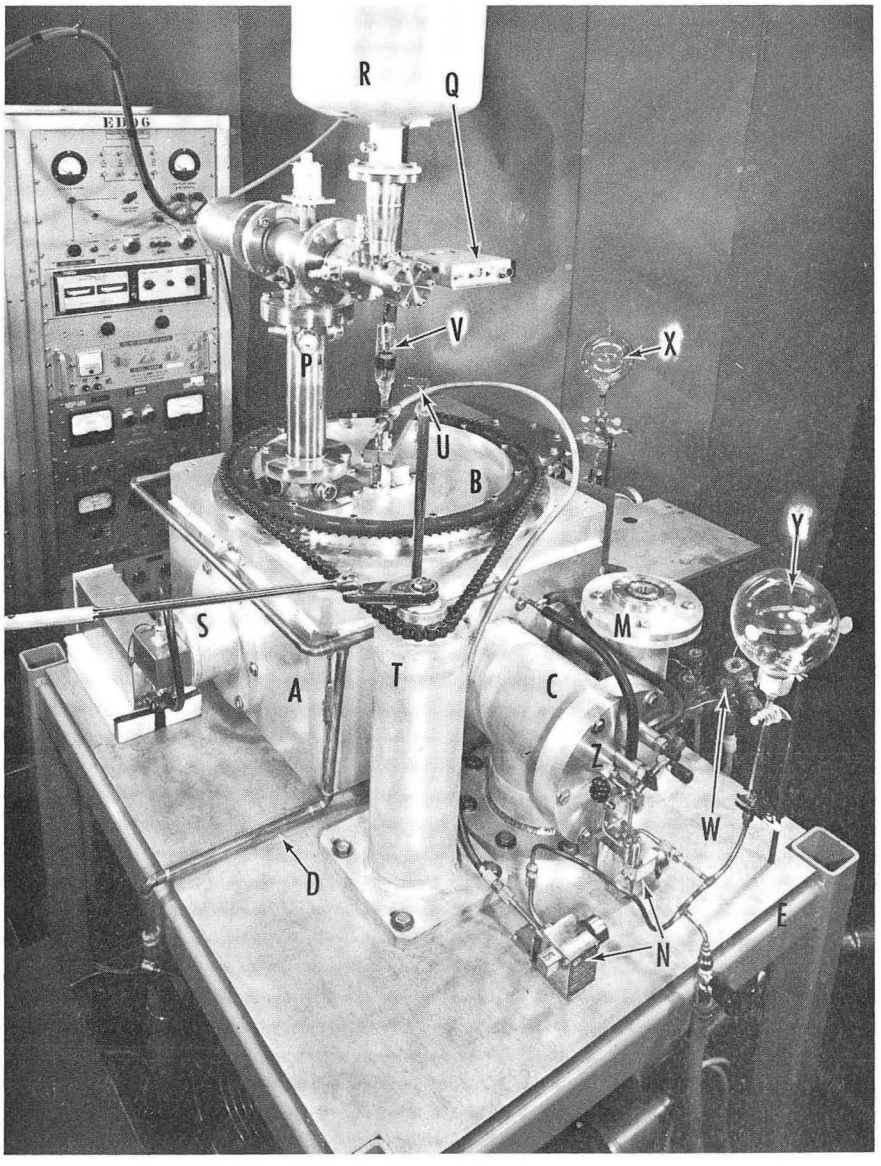

XBB 670-5733

Fig. 5.

$1\text{-}2\times10^{-7}$ torr. Interlock circuits automatically shut off power to the diffusion pumps and set off an alarm if the forepump pressure or the flow rate or temperature of the cooling water stray outside preset limits. The permanent gas pumping rate is estimated to be about 1500 liters/sec for air. Very efficient cryogenic pumping for condensable gases is provided by a large cylindrical liquid nitrogen cooled copper cold shield which entirely surrounds the scattering region except for holes where the beam source components protrude through. Differential pumping for the double tec-ring seal of the rotatable lid is done through the tubing D.

The main chamber and its associated diffusion pumps and water and power connections are supported by a tubular steel frame E. A carriage slips under this frame and lifts it for minimum inconvenience in moving, although one would certainly not describe the apparatus as portable. The frame can also support a demountable crane which is used in removing the lid of the main chamber.

The ion source F is mounted on a separate vacuum chamber G, which is also equipped with a six-inch oil diffusion pump. The high pumping speed is necessary to keep the background pressure at about 10^{-6} torr while the ion source is operated at 10^{-3} torr. The efficient differential pumping between the main chamber and the ion source also prevents the target gas from leaking into the ion source.

The ion source is coupled to the main chamber by the magnetic mass spectrometer chamber H, which passes between the poles of the magnet I. The ion extraction and initial focusing elements are mounted inside the ion source vacuum chamber, and the final focusing elements and beam defining slits are mounted inside the main chamber on the flange J. The level of the ion source vacuum stand may be adjusted relative to

the main chamber by means of the screws which attach the stand to its carriage.

All the electronics necessary for the day-to-day operation of the equipment is housed in three 72" double racks or located on the apparatus itself, except for some recorders, the high voltage power supply, and the Teletype data printer and tape punch associated with the ion counter.

CHAPTER III

Detailed Descriptions of Components

This chapter will be devoted to discussing the construction and operation details of the various components of the apparatus which have already been built and tested, in the light of what each component is required to do in the complete system. In addition an attempt will be made to show how future modifications were planned for and how they will increase the capability of the apparatus.

A. Main Chamber

The features desired in the main chamber were a fast pumping speed for both condensable and noncondensable gases, convenient facilities for mounting and precisely aligning many different beam source and detection components, and easy and accurate rotation of the detectors under high vacuum. The way our design meets these specifications can be seen from Fig. 6.

The chamber is constructed of type 6061-T6 aluminum alloy slabs. These were first roughly machined to size and tack-welded together at the seams, then welded vacuum-tight on the inside of the chamber to avoid fissures where hard-to-remove contaminants could accumulate. The final machining of the critical surfaces was done after the completion of all welding.

Access to the chamber is through a 7" diameter port in the center of each vertical face, and through ports in the rotatable lid of the chamber. To make alignment of the beam and detection components simple and accurate the external surfaces were required to be flat within 0.005" overall. Opposite faces are parallel and adjacent faces per-

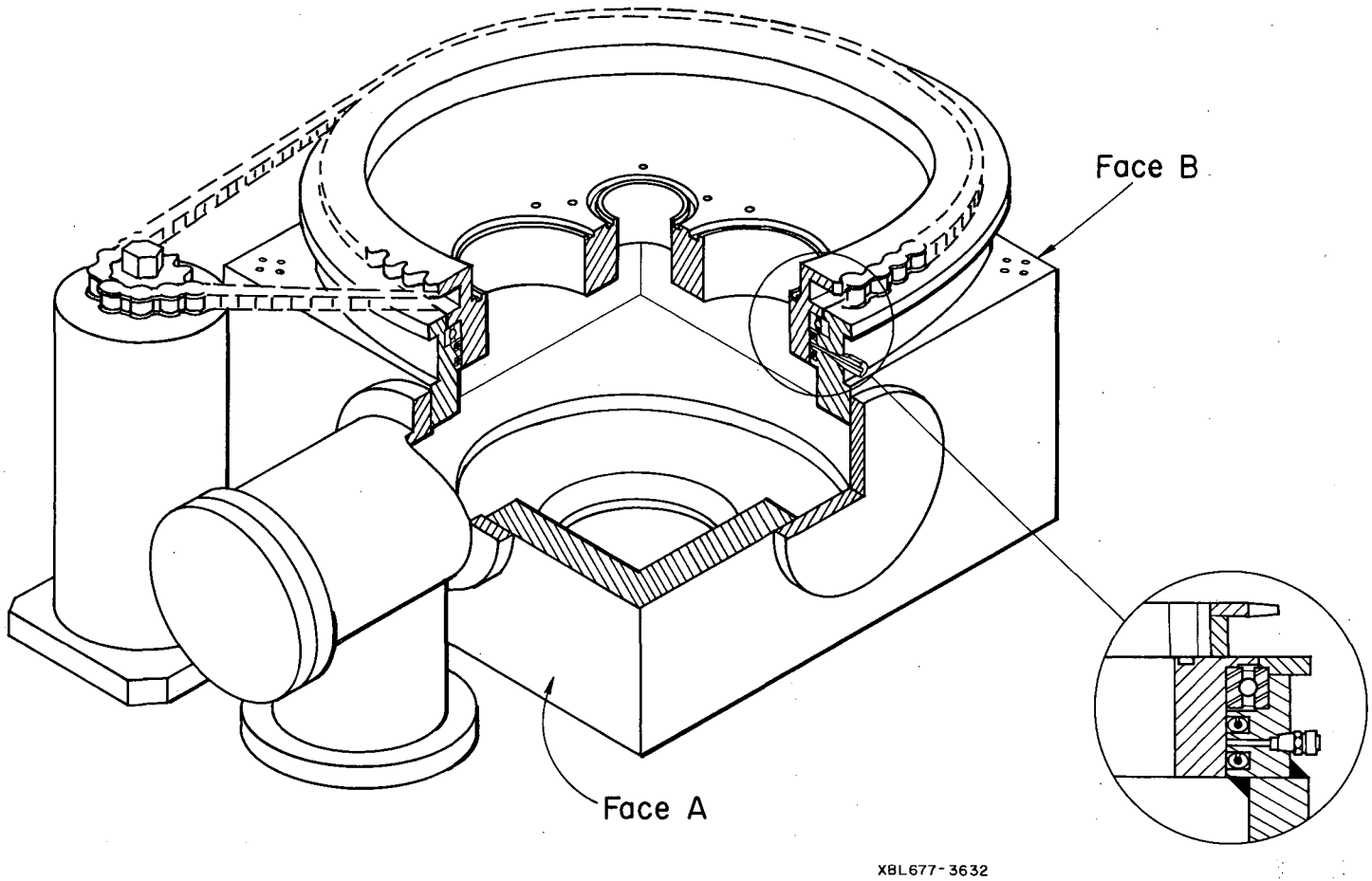

Fig. 6. Main chamber. Inset shows detail of tec-ring seal.

pendicular within 0.005" overall, and the side ports are located on intersecting centers within 0.005". In addition horizontal and vertical lines were inscribed to mark the exact center of each port to aid in alignment. The 5" diameter ports in the rotating lid are located within 0.003" of perpendicular lines intersecting the center of the chamber. The degree graduations around the circumference of the lid correspond to the locations of these holes within 0.003". Dowel pin holes were accurately drilled at each of the main chamber ports, in case the component to be mounted required very accurate angular alignment.

The inset in Fig. 6 shows the details of the ball bearing support and double tec-ring seal for the rotating lid. The ball bearing* provides the only support for the weight of the lid plus the pressure difference, the sum of which is a force of about 5000 lb. when the chamber is evacuated. The tec-rings† are made of precision machined teflon, with a Buna-N rubber core to give compressibility. The space between the tec-rings is pumped out by a small mechanical pump through the ports shown. The performance of this seal has been excellent, although the tolerances suggested by the manufacturer for the tec-rings were found to be too lax and it was necessary for us to choose the best of those available. After several months of operation tiny pieces of teflon, which peal off the rings due to friction, roll up between the sealing surfaces and cause leaks. This necessitates removing the chamber lid and cleaning and reinstalling the tec-rings. A thin coating of Apiezon N vacuum grease seems to make the tec-ring seal last a little

* Supplied by Kaydon Engineering Corp., Muskegan, Michigan.

† Supplied by Tec Seal Corp., Wilmington, Calif.

longer between cleanings, probably due to the fact that it can fill the first small leaks which occur. This need for periodic maintenance cannot be regarded as an important disadvantage, since it only requires shutdown of the apparatus for one day every four to six months. When the tec-rings are clean no increase in pressure perceptible with the ion gauge on its lowest range (10^{-6} torr full scale) occurs when the lid is rotated. Despite the large force on the lid and the friction of the tec-ring seal, the 7-to-1 reduction on the chain and sprocket drive enables the lid to be rotated easily. Screw holes in the chamber are provided for the mounting of brackets used in removing and installing the lid, and for eye bolts used to support the lid with a portable crane. The screw holes for the main flanges and all other frequently used tapped holes in aluminum or copper are reinforced with stainless steel Heli-Coil inserts.

As noted in the previous chapter, the main chamber is pumped by two 6-inch oil diffusion pumps, of which one is located so as to be able to provide differential pumping for the neutral beam before the intersection with the ion beam if the source is mounted on face A, or after intersection with the ion beam if the source is mounted on face B. Additional pumps may be added to the other side ports if needed for a particular application. The copper cold shield, which rests on three stainless steel screws, is cooled by liquid nitrogen from a dewar mounted on flange M (Fig.). A hole in the cold shield at each chamber port allows beam source and detection components to protrude through. Blank plates are used to cover the holes when the corresponding ports of the chamber are not in use. A 25-liter charge of liquid nitrogen is sufficient to keep the shield cold for several days once it is initially cooled. The

temperature of the shield is monitored by means of two iron-constantan thermocouples on opposite sides of the chamber.

B. Ion Beam Sources, Focusing System, and Monitors

1. Electron Bombardment Source

The electron bombardment ion source is similar in principle to one described by Carlson and Magnuson.[18] This type of source was chosen because of its usefulness with a large number of gases, its stability, and its high ion current yields at relatively low source pressures. The last feature makes the job of differential pumping fairly simple. A cutaway drawing of the ion source is given in Fig. 7, and a photograph of the assembly is shown in Fig. 8.

A low voltage AC current is used to heat the filament A, and the emitted electrons are drawn through the 1/8" diameter aperture in the plate B into the anode C. A solenoid consisting of 2500 turns of 24-gauge copper wire imbedded in epoxy resin is wound around the anode. The DC current passed through the solenoid sets up an axial magnetic field which confines the electrons to helical paths of small radius. The electrons are repelled as they approach either of the electron reflection plates B or D. Thus they continue to oscillate between the plates until they finally reach the wall of the anode and are captured. The energy of the electrons in the potential well of the anode is determined by the relative DC potentials applied to the filament and to the anode and by the distribution of space charge within the anode. The gas to be ionized is admitted to the source through the capillary tube E and the flow rate controlled with a Granville-Philips Variable Leak valve. Ions created by impact of the electrons on the gas molecules are extracted axially through the 3/32" diameter aperture in the plate D.

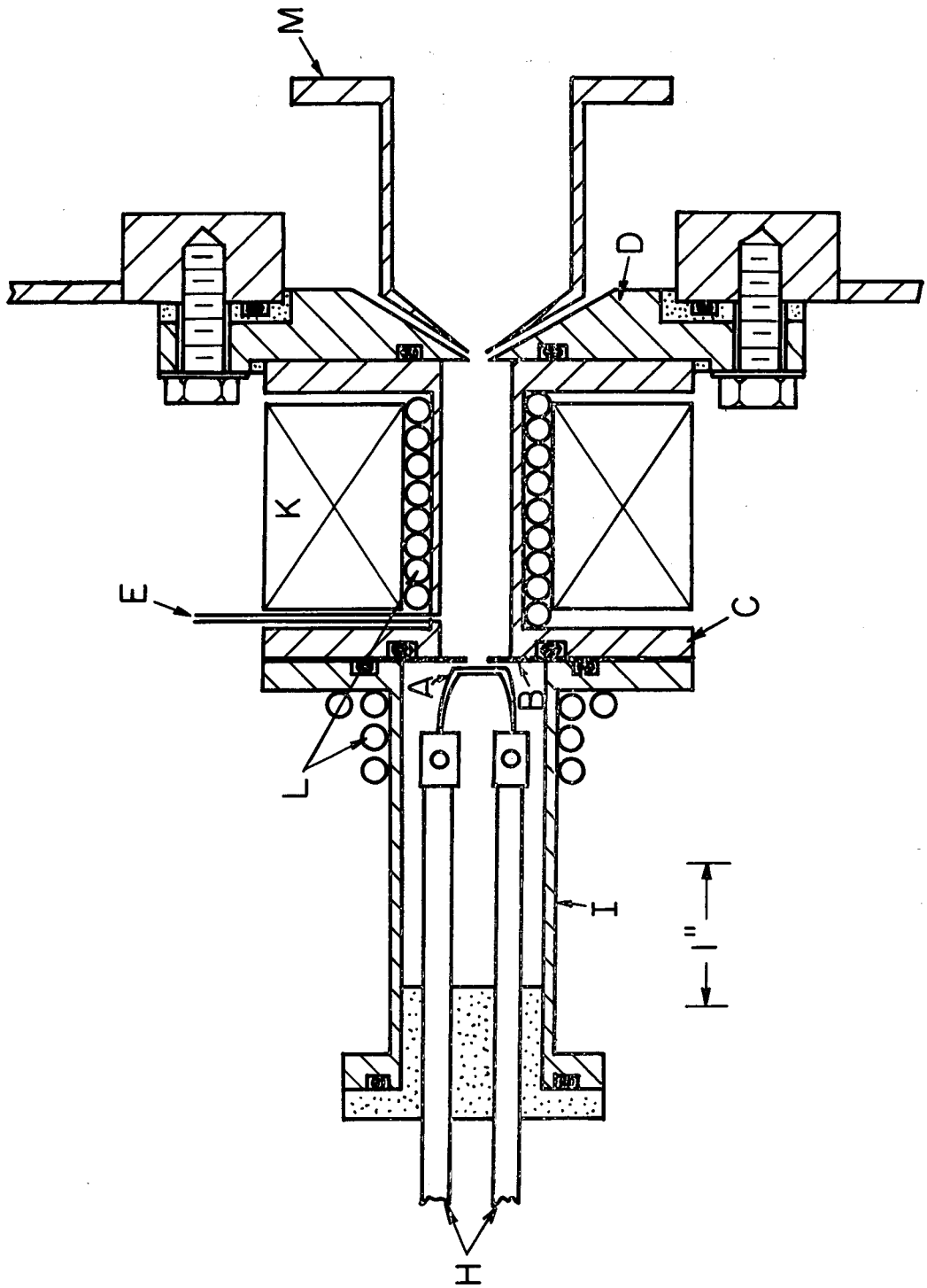

XBL677-3633

Fig. 7.

Fig. 7 Electron impact ion source.
Index applies to both Figs. 7 and 8.

A Filament

B Electron reflection plate

C Anode

D Electron reflection plate

E Gas inlet capillary

F Differential pumping chamber ion gauge

G Focusing element electrical feedthrough

H Filament electrodes

I Filament chamber

J Hastings gauge

K Solenoid

L Water cooling lines

M Extractor cone

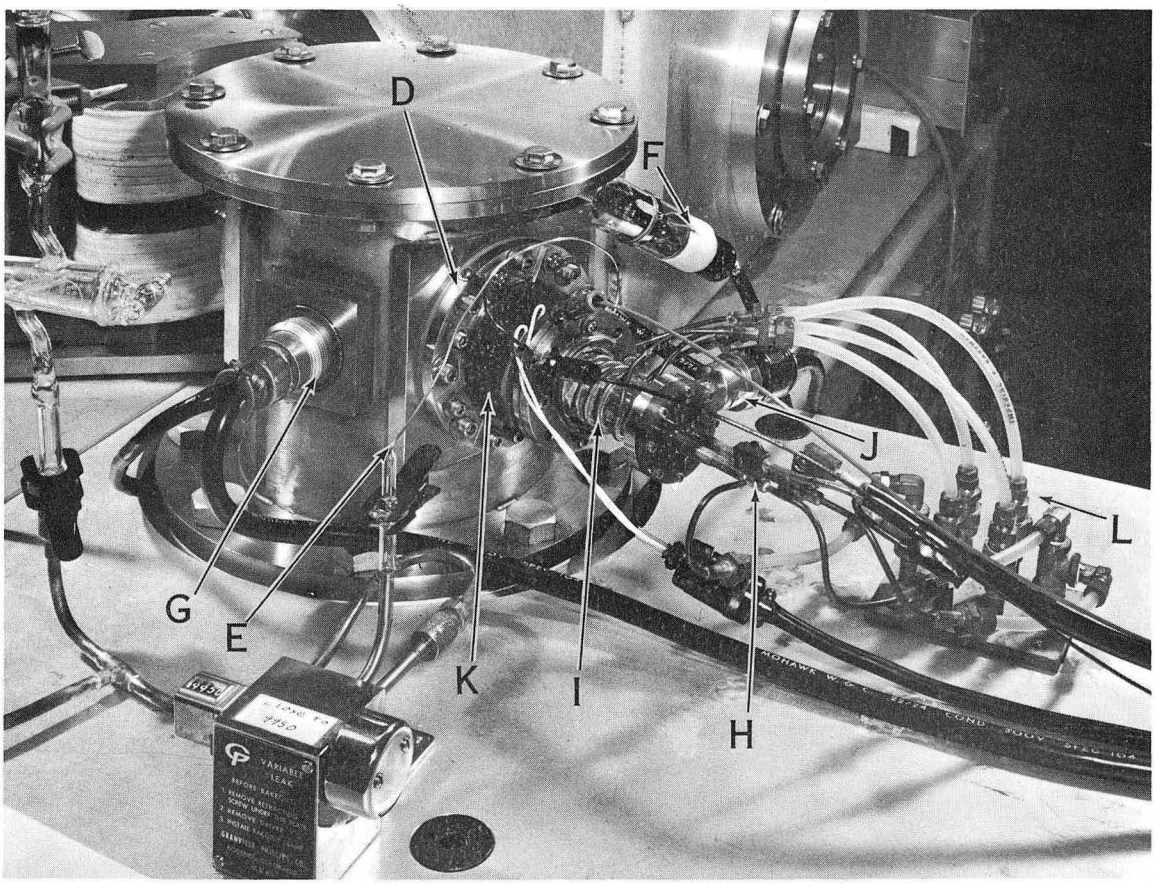

XBB 670-5732

Fig. 8. Photograph of electron bombardment ion source.

The filament chamber I, the anode and the plate D are constructed of non-magnetic stainless steel (type 316 or 304), and are water-cooled by means of copper tubing wound around the outside and soft-soldered for good thermal contact. The filament electrodes are made of copper, with molybdenum tips and screws to hold the filament. The electrodes are imbedded with epoxy resin in Nema (a fiberglass-epoxy composition with good vacuum properties and capable of withstanding high temperatures) and are water cooled. The filament is about 5 cm of 20 mil diameter tungsten wire non-inductively wound in a plane parallel to the electron reflection plate B. So far, only tungsten filaments have been used, but a platinum or iridium filament would be advisable if the source is operated with oxygen-containing gases. Because of the proximity of the hot filament, plate B is made of molybdenum. Viton O-rings are used in the ion source because of their superior performance at high temperatures. Mylar insulators of 3 mil thickness are placed between the plates B and D and the anode. Other insulation is shown in the drawing.

In operating the source, the filament is first heated, then the DC potentials are applied, gas is admitted to the anode, and the electron energy and solenoid current adjusted to give the maximum emission. A Hastings gauge is provided to read the source pressure in the filament chamber, but in general the pressure at which the source is operated (about 10^{-3} torr) is below the useful range of this gauge. This necessitates monitoring the source pressure by means of the ion gauge in the differential pumping chamber, which has a pressure about a factor of 1000 (determined by the conductance of the extraction aperture) lower than that of the source. The residual pressure in the differential pumping chamber is below 10^{-7} torr. When the source is operating the

differential pumping chamber pressure is set between 1 and 2×10^{-6} torr.

Over a period of several months, oxide deposits from the residual air in the source will build up in the anode and on the electron reflection plates, causing the performance of the source to deteriorate. When this occurs, the original condition may be restored by dissembling the source and abrading off the deposits. The filament life is unknown, since none have yet failed in the course of normal operation.

We have tested the source with Ar, He, N_2, CH_4 and H_2, and have produced stable beams with space-charge limited intensity of Ar^+, He^+, N_2^+, CH_4^+, CH_3^+ and H_2^+, as well as lower intensities of doubly charged ions, N^+, CH_5^+ and H^+. The usefulness of the source presumably extends to many other gases.

2. Alkali Metal Ion Source

For alkali metal ion beams a thermal ionization source, shown in Fig. 9 is used. The source operates on a principle discovered by Kingdon and Langmuir[19] in 1923 - namely, that a large fraction of atoms will be ionized when evaporating from a clean metal surface whose work function is greater than the ionization potential of the atom. Since only refractory metals can be heated to sufficient temperatures to remove surface contaminants, and since the surface work functions of these metals are low (4.58 eV for tungsten[20]), only the alkali metal ions K^+, Rb^+ and Cs^+ can be created with great efficiency by this method.

The source employs a 0.250" diameter porous tungsten button* A in the end of a molybdenum tube B. The button is heated by a noninductively wound 20 mil tungsten wire which is alundum coated and covered with a

* Supplied by Semicon Associates, Inc., Lexington, Kentucky.

Fig. 9 Thermal ionization source for alkali metal ions

A Porous tungsten button

B Molybdenum tube

C Reservoir

D One of three 50 W cartridge heaters

E Nylon insulator

F Button heater and radiation shield

G Stainless steel bellows

H Asbestos and glass wool insulation

I Heater leads (tantalum)

J Thermocouple leads

K Wafer cooling coils

L Copper gasket

M Steel set screw

N Ion source vacuum chamber flange

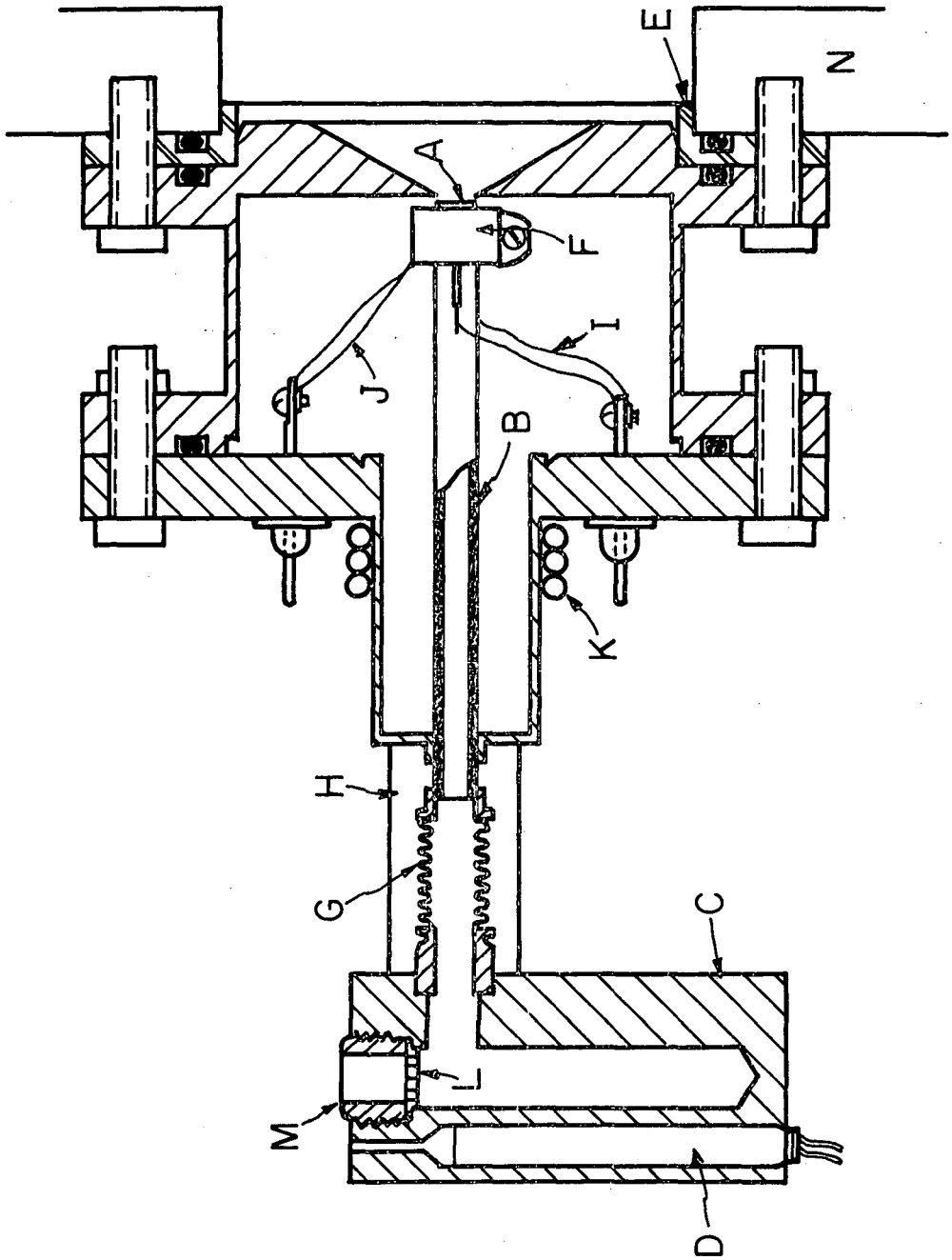

XBL677-3634

Fig. 9.

tantalum radiation shield. Tantalum wires connect the heater to the vacuum feedthroughs, and a Pt-90% Pt,10% Rh thermocouple is used to monitor the button temperature. When the reservoir C containing the alkali metal is heated by three 50W cartridge heaters (e.g., D) the vapor diffuses to the heated button and is ionized. The reservoir is made of Type 304 stainless steel and is sealed by tightening a hardened steel set screw against an annealed copper gasket. Asbestos and glass wool insulation is used to keep the material evaporated from the reservoir from condensing in the stainless steel bellows which connects the reservoir to the ionizer tube. The source, all of which is floated at a potential equal to the final desired ion energy, is electrically insulated from the differential pumping chamber by a precisely machined nylon gasket E and by mylar washers on the screws of that flange.

The electronics needed to operate the source are a filtered DC power supply for the tungsten button heater (~10 amp, 15V) and a Hallikainen "Thermotrol" temperature regulator (±0.1°) for the reservoir. The regulator is controlled by a platinum resistance thermometer imbedded in the nickel block.

Beginning with the removal of the previous alkali metal from the reservoir, the source is prepared for operation as follows: The tungsten button is baked out for an hour or so with the reservoir cool in order to evaporate any deposits of alkali metal. The button is then cooled, the source removed from the vacuum system, and the reservoir washed with dilute acid and rinsed with alcohol. Care must be taken not to contaminate the tungsten button by touching it with the fingers or clogging it with alkali metal hydroxides. After the assembly is thoroughly dried in a 60°C oven, the reservoir is loaded with several grams of the desired

material in a dry nitrogon atmosphere, and sealed. The source is then replaced in the vacuum system, which is immediately pumped down. When a pressure of less than 10^{-6} torr is achieved, the button is baked out for an hour to remove contaminants and any remaining traces of the previous alkali metal.

After the extraction voltage is applied, the button is heated to 1200°C (requiring about 100 watts of power from the heater coil). The reservoir temperature is then raised until the vapor pressure of the metal is sufficient to give adequate emission. One gram of material lasts for many hundreds of hours at the total emission currents used, which were always less than 1 ma. In shutting down the source, the reservoir is cooled first to allow the material in the vicinity of the tungsten button to recondense, then the button is slowly cooled with the extraction voltage still applied. No maintenance other than the occasional replacement of the heater wire has been necessary. The source yields space charge limited beams of K^+, Rb^+ and Cs^+.

3. Ion Beam Analysis and Focusing System

The ion beam focusing and analysis system should give beams of high intensity and stability, small energy spread and angular divergence, and good mass separation over the entire range of desired energies. Because better energy resolution was desired in the final beam than could easily be obtained directly from the ion source, the beam handling system includes a magnetic momentum analyzer, with resolution dependent on the entrance and exit slit dimensions.

Two electrostatic focusing stages are used: the initial focusing stage extracts the ions from the source and focuses them into the entrance slit of the momentum analyzer, and the final focusing stage takes

the ions exiting from the analyzer and forms them into the final beam. Initially, during the alkali metal charge transfer measurements, two series of cylindrical lenses, shown schematically in Fig. 20 were used for the initial and final focusing. A much more efficient and versatile focusing system employing quadrupole lens pairs was then installed and will probably be used exclusively in the future. This focusing system is shown schematically in conjunction with the electron bombardment ion source in Figs. 10 and 11.

The focusing system is divided into three regions separated by the parallel grid pairs E and L which decouple the focusing in one region from that of the next regardless of their relative basis potentials provided the ions travel between the regions perpendicular to the grids. In the first region the conical element A extracts the ions from the source and the double aperture lens B forms them into a roughly parallel beam. The element C serves to skim off all except the usable central portion of the beam and is shaped so as to prevent buildup of a large space charge at this point. The einzel lens D corrects the focusing just before the beam enters the analysis region. The parallel grids E are used to accelerate or decelerate the ions to the energy desired in the analysis region. Up to this point the ion beam is cylindrically symmetric. Because the magnet focuses ions only in the horizontal plane, however, it is desirable to electrostatically focus the beam in such a fashion that the ion velocities have no vertical component, but converge in the horizontal plane into the entrance slit of the mass spectrometer chamber G. In this way ion intensity is not lost due to vertical spreading of the ion trajectories in the analysis chamber. To accomplish this the electrostatic quadrupole lens pair F takes the

Fig. 10 Ion beam focusing and analysis system schematic (Horizontal section) shown with electron bombardment ion source

A Extraction core

B Double aperture lens

C Skimmer

D Einzel lens

E Parallel grid pair

F Initial focusing stage quadrupole lens pair

G Mass spectrometer chamber

H Magnet poles

I Support flange

J Shield

K Final focusing stage quadrupole lens pair

L Parallel grid pair

M Einzel lens

N Final slit

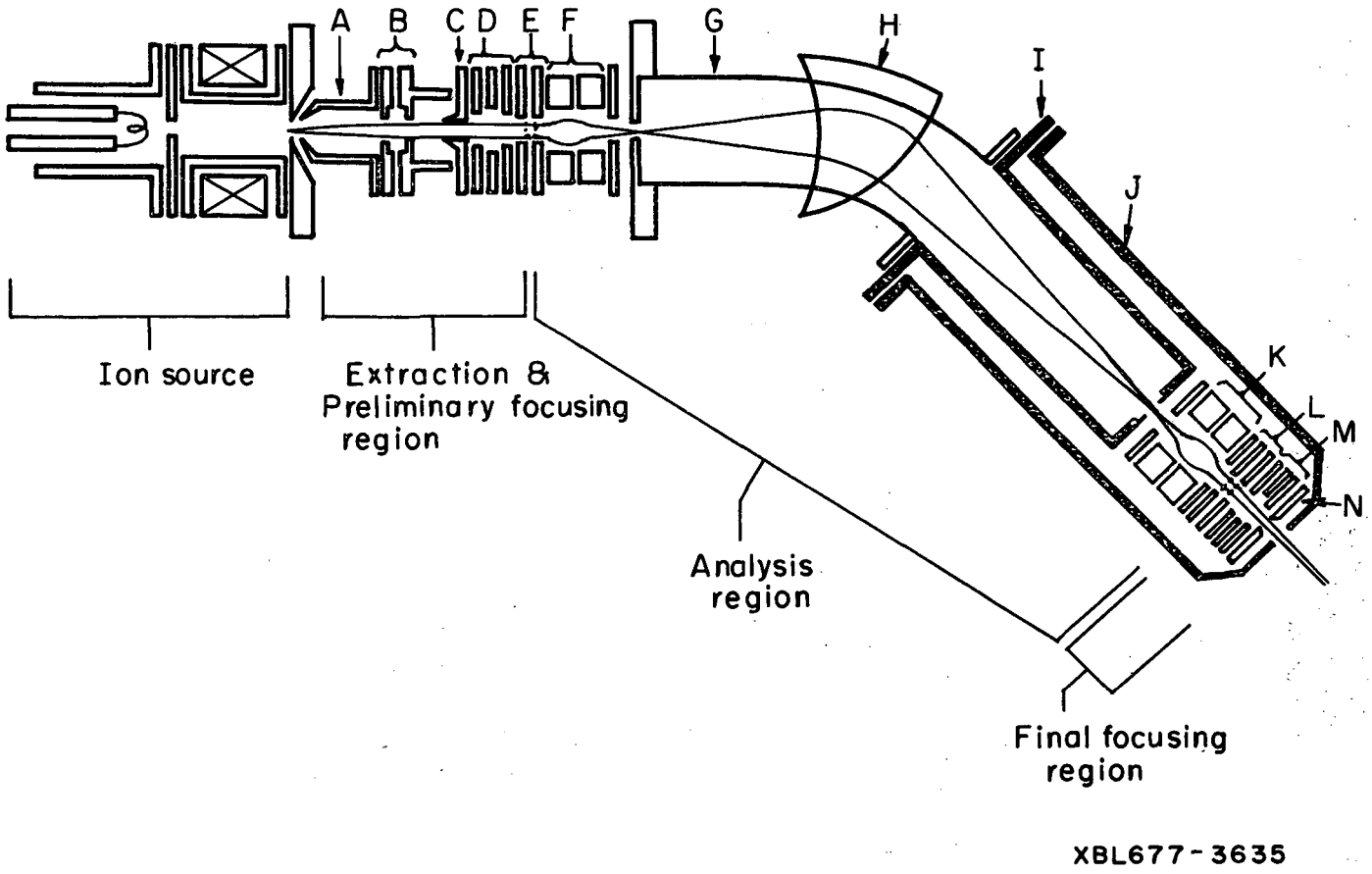
A
B
C
D
E
F
G
H
I
J
K
L
M
N
Ion source
Extraction &
Preliminary focusing
region
Analysis
region
Final focusing
region
XBL677-3635

Fig. 10.

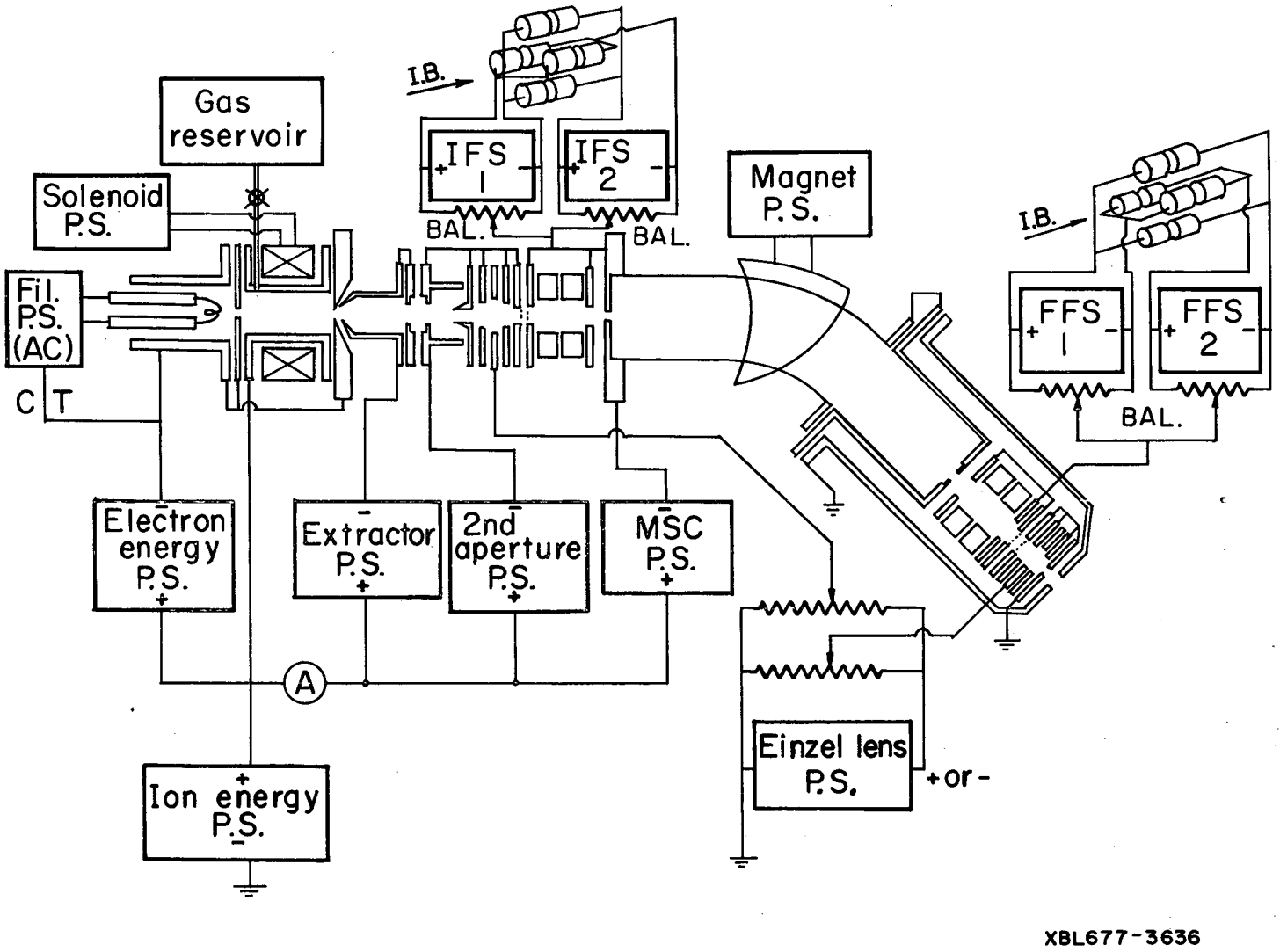

Fig. 11. Ion beam focusing and analysis system (horizontal section) block diagram of power supply connections.

collimated beam of square cross section as it emerges from the parallel grids and converts it into a line-focused beam as shown in Fig. 10. The beam then passes between the poles of the electromagnet H, where the ions are separated according to their momenta. The line-focused beam emerging from the exit slit of the mass spectrometer chamber is reconverted into a collimated beam by the electrostatic quadrupole lens pair K, is accelerated or decelerated to its final energy by the parallel grids L, and correctively focused if necessary with the einzel lens M. It then passes through the final defining slit N into the main chamber.

Design Features

The double aperture lens dimensions were calculated from graphical relationships between parameters given by Spangenberg.[21] An approximately four-to-one ratio of first and second aperture potentials with respect to the ion source will collimate a beam with point origin at the exit aperture of the ion source.

The quadrupole lens pairs were designed according to criteria given by Lu and Carr[22] for interconversion of line-focused and parallel beams. Important constraints are the dimensions into which the lenses must be fitted, the desired final beam dimensions, and the acceptance angle of the magnet. The quadrupole lens design is not coupled to the momentum analyzer slit widths, which may be varied according to the resolution required, but the two quadrupole lens pair dimensions and operating voltages are coupled to each other and to the ratio of image to object distance for the magnet since the second lens must exactly undo the divergence of the beam through the mass spectrometer exit slit. The quadrupole lenses perform as expected except that they require operating voltages roughly a factor of two higher than the theoretical values.

The initial and final electrostatic focusing stages are supported by sets of four rods screwed into chambers G and I, respectively. The elements are mounted on nylon insulators which fit tightly over the support rods. Tolerances of 0.0005" are maintained on the mounting hole locations to insure accurate alignment of the elements. The support rods and the lens elements which are exposed to high ion currents are made of type 304 stainless steel; the other elements are made of aluminum. All of the lens elements and the chambers G and I are polished and gold-plated to insure clean, conductive surfaces throughout the ion beam path. The grids are 80%$^{+}$ transmission gold mesh with 100 wires to the inch.

The momentum analysis magnet shown in Fig. 12 was designed with the aid of an instrument described by Walton[23] for determining the correct field exit boundary shape to give high order focusing for a given entrance field boundary. The criteria used in the design were that the ion trajectories should be incident normal to the field boundary, that the energy dispersion should be large, and that the image and object distances should correspond to convenient apparatus dimensions. The dimensions chosen were 12 cm for the image distance, 24 cm for the object distance, and a 66° ion deflection angle. A cylindrical surface was used to approximate the exit field boundary, and half of the 5/8" pole separation was assumed for the fringing field correction. With 2mm entrance and exit slit widths the momentum spread in the analyzed beam is 1.5%. It is important for some experiments that, since the energy spread of the beam emerging from the ion source is small, the magnetic momentum analysis achieves mass separation also.

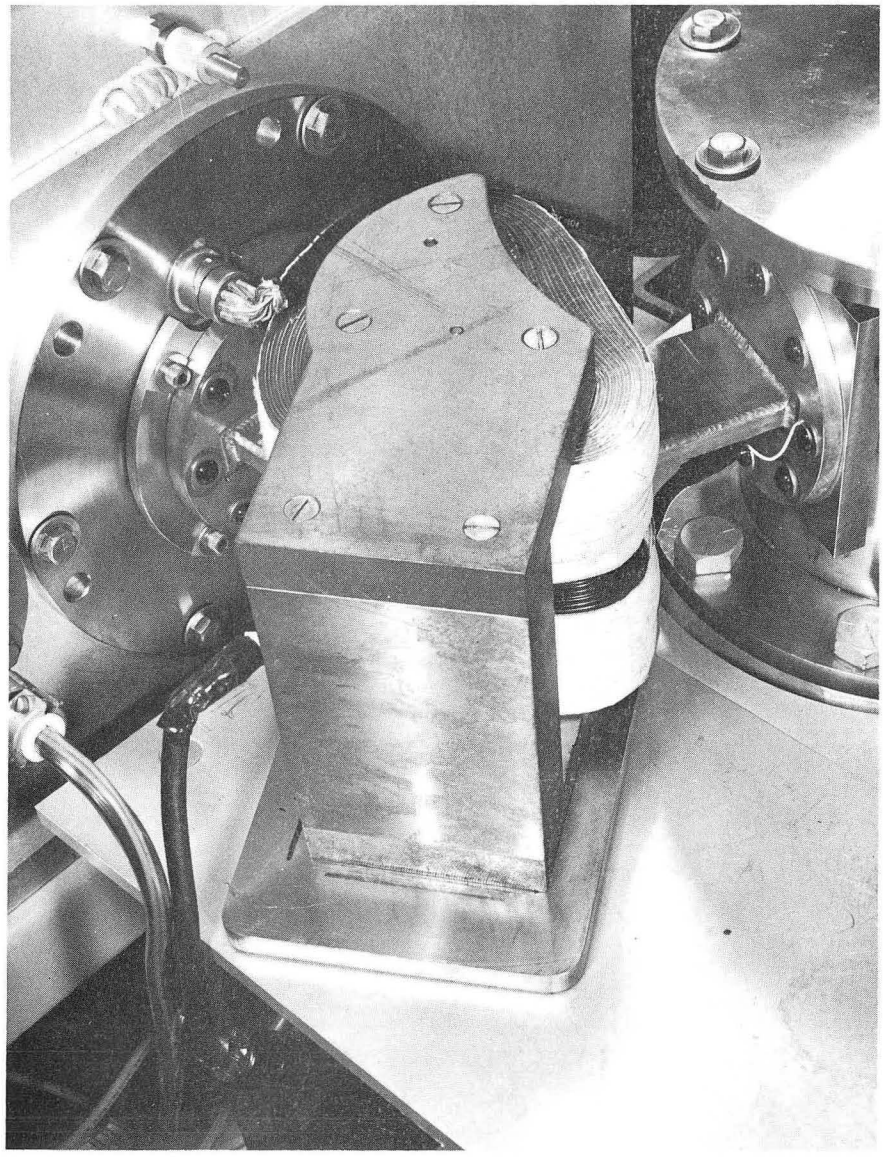

XBL 677-3596

Fig. 12. Ion beam analysis magnet

The magnet is machined of hard roll steel and powered through 1000 turns of 14 ga. copper wire wound in two coils near the gaps and imbedded in epoxy resin. The current required is given by

$$i_{Magnet}(amp) = \frac{\sqrt{M_i E_i^a}}{44} \qquad (11)$$

where M_i is the mass of the (singly charged) ion in a.u. and E_i^a is the energy of the ion in the analysis chamber in eV.

Operation

A schematic of the power supply connections for the ion source and focusing system is shown in Fig. 11. All of the interconnections are made in a central control panel. Except for the einzel lens potentials, which are referenced to ground, all of the power supplied are floated at the potential of the ion source anode with respect to ground, which determines the final ion energy. Thus the ion energy may be varied without changing the relative focusing voltages or the energy of the ions in the analysis chamber.

An extraction voltage of 200-300 V is generally used, with a second aperture potential of 50-60 V. The energy at which the ions are momentum analyzed is chosen as a compromise between resolution and intensity and depends on the requirements of the particular experiment. The feature which allows the analysis energy to be selected independently of the final beam energy is especially convenient for low energy experiments, where disastrous space charge spreading is avoided by retarding the ions to their final energy at the last grid pair, less than 4 cm from the interaction region.

The quadrupole and einzel lens potentials are adjusted to give the optimum intensity and profile shape in the final beam. The einzel lenses give convergent focusing for center element potentials either positive or negative with respect to the outside element potentials, but are usually operated with negative potentials. Balance helipots (see Fig. 11) are provided for the quadrupole lens positive and negative voltages, but symmetric potentials are almost always used.

4. Ion Beam Monitors

A large Faraday cup installed opposite the ion beam exit slit is used to monitor the total ion beam current in crossed beam experiments. This cup is shown in Fig. 20. In addition, other cups may be used for special purposes. Faraday cups with very small apertures have been mounted in the rotatable lid for measuring the primary beam angular distribution, and cups equipped with parallel retarding potential grids have been used for energy analysis of the primary beam and for calibration of the detector energy analyzer. The cups are long and narrow to minimize the escape of ions by elastic scattering, and may be biased through the electrometer at potentials which are either positive (to prevent the escape of secondary electrons) or negative (with alkali metals, to prevent the escape of ions created by surface ionization).

C. Neutral Gas Targets and Monitors

1. Collision Cell

The collision cell is shown mounted in the center port of the main chamber rotatable lid in Fig. 13. The cell consists of two concentric cylinders; the inner cylinder contains the ion beam entrance aperture (2mm × 2mm) and is held stationary, while the outer cylinder contains the product ion exit aperture (also 2mm diameter) and rotates with the

Fig. 13 Collision cell. Cutaway shows inner cylinder and rubber gasket seal

A Outer cylinder (rotatable)

B Inner cylinder (fixed)

C Ion beam entrance aperture

D Product ion exit aperture

E Rubber gasket

F Slot cut in inner cylinder to allow escape of ions in 110° span

G Gas supply tube

H Wilson vacuum seal

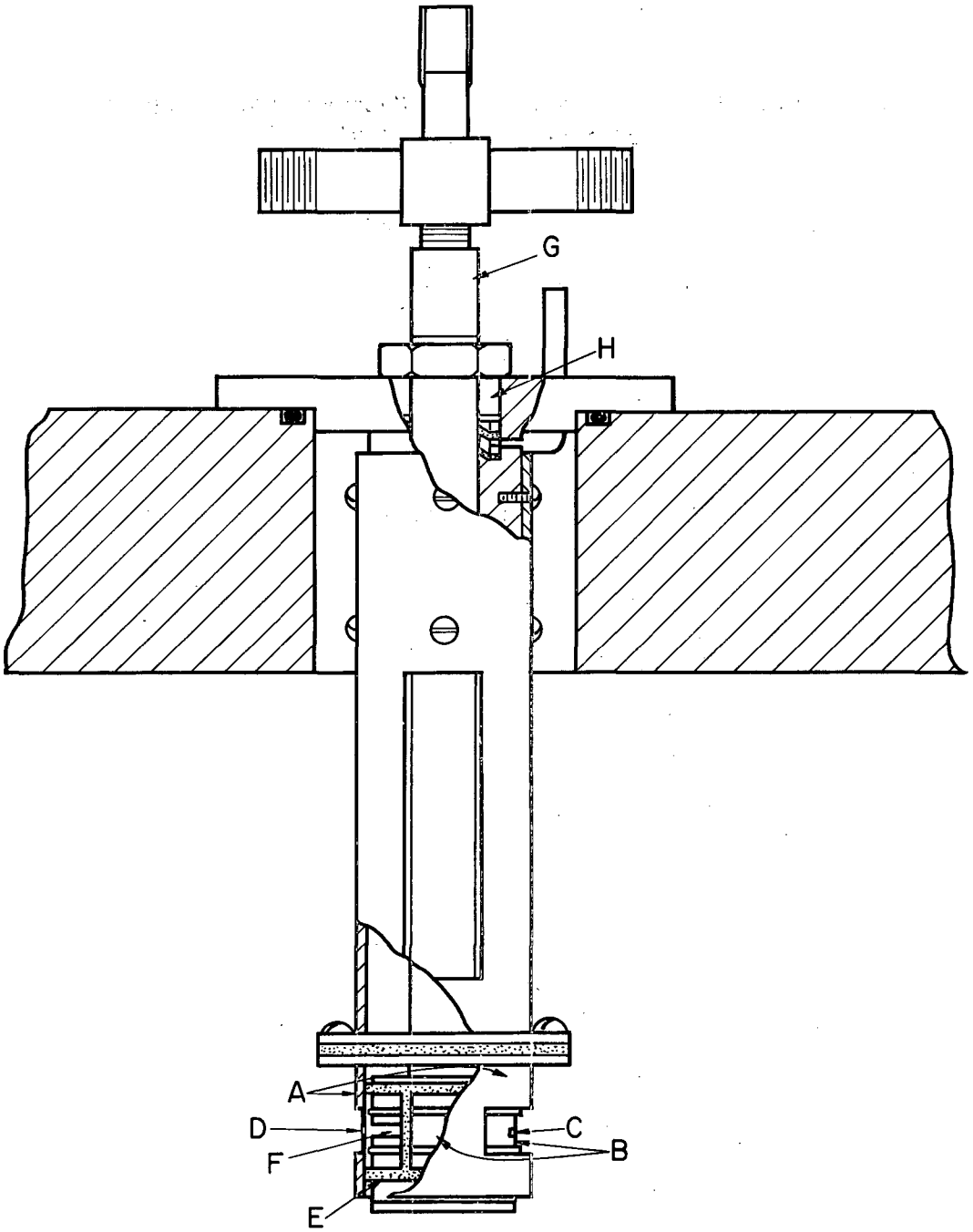

Fig. 13.

detector. The gap between the two is sealed by rubber gaskets. The radial distances from the center of the collision cell to the entrance and exit apertures are 0.63" and 0.88" respectively. Slots cut in both cylinders allow rotation of the exit aperture through a total of 110° without blocking either opening. Gas is admitted to the cell through the center tube, which passes through a Wilson seal to allow rotation. The pressure is monitored at the top of this tube by an ionization or other gauge. A Granville-Philips Variable Leak valve is used to adjust the flow rate to the cell from a 1-liter flask at about 1 atm. pressure. About 2 ml/hr is consumed.

The ratio of the main chamber pumping speed to the conductance of the apertures is sufficient to maintain a main chamber pressure a factor of 1000 lower than the collision cell pressure. This provides a very favorable signal-to-background ratio by Eq. (2), taking b equal to the collision cell diameter. The inside and outside of the collision cell are thoroughly coated by painting with a colloidal graphite dispersion to reduce the possibility of surface charge buildup. The collision cell is machined entirely of Type 304 stainless steel except for the mounting flange.

2. Nozzle Source for Alkali Metal Beams

In the earliest alkali metal experiments, a neutral beam oven with a Zacharias "crinkly foil" slit was used, but this source failed to give sufficient intensity. A nozzle source was then constructed which proved very satisfactory. The design was guided by Hundhausen and Pauly's[32] description of a similar source employing a circular nozzle. Figure 14 shows the oven with the Laval slit attached, and Fig. 20 shows how the source is mounted in the vacuum system.

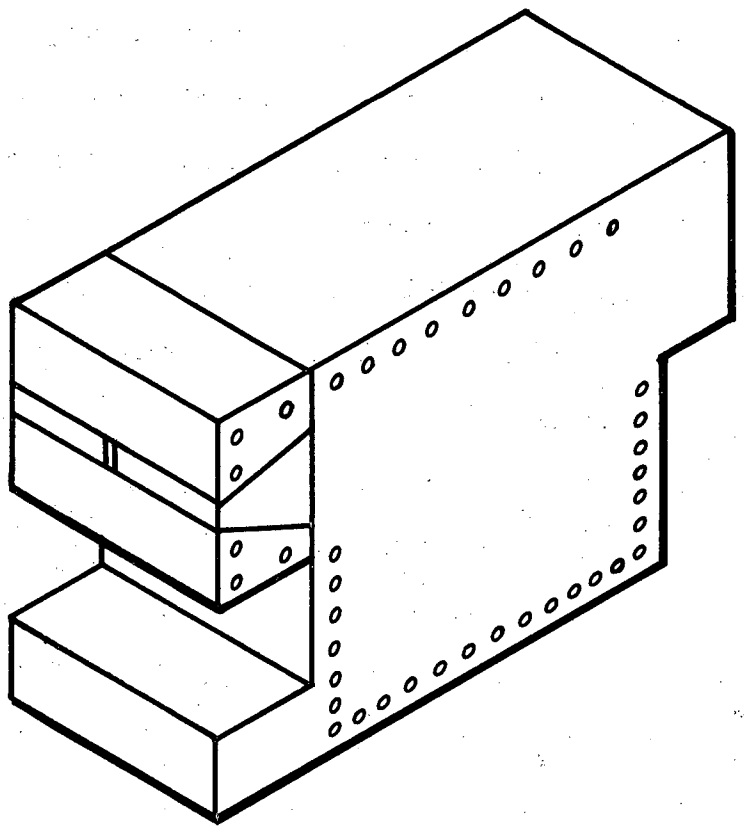

XBL677-3638

Fig. 14. Alkali metal nozzle beam source.

The oven and the slit are machined of pure nickel and are heated by a wire passing through thin alumina insulators inserted in holes around the periphery of the block. An iron-constantan thermocouple is used to monitor the oven temperature. The oven is sealed by tightening a steel set screw against an annealed copper gasket. Because it was important in the determination of the absolute cross sections to have the neutral beam density be uniform over the vertical height of the ion beam, a long narrow slit was used instead of a circular nozzle. The optimum intensity to consumption rate ratio was found to be with the 0.250" high slit adjusted to a width at the minimum of 0.004".

Contrary to the case with permanent gases, a nozzle source for alkali metal beams is quite easy to construct and operate because of the very large pumping speed of a cryogenic surface for these materials. The arrangement used is shown schematically in Fig. 20. The source oven is mounted on quartz insulators and is supported by a bar from the side flange of the chamber. The oven is surrounded by a liquid nitrogen cooled copper cold shield which screws onto the main cold shield. The first slit after the source is also liquid nitrogen cooled and serves to skim off all but the center of the beam. The next slit is heated to prevent condensation and is used to actually define the beam width, this slit being slightly narrower than the previous cold slit. Following the hot slit are shielded electrodes used to deflect charged particles from the beam. The beam may be interrupted between the source and the cold slit by means of a manually operated flag.

Because of the large amounts of alkali metal consumed (1 to 2 g/hr) the cold shield must be cleaned and the source reloaded for each day's operation. In order to avoid wasting material, the oven is heated rapidly at first then the power is decreased to just that amount (about 30 watts) necessary to keep the temperature stable at the desired value, where the vapor pressure of the alkali metal is 2-4 torr.

3. Multichannel Beam Source

The multichannel source is mounted in the main chamber tee as shown in Fig. 15. The slit* is a fused array of glass capillaries 7 microns in diameter and 0.010" long with a 58% open area, which mounts on the end of the chamber A as shown. The short channel length allows the source to be operated efficiently at pressures of several hundred microns (see Chapter 1). Gas is fed in by the Granville-Philips Variable Leak valve B through a flexible stainless steel bellows into the tube C. The position of the source can be adjusted with the screw D. This permits the intensity versus the angular spread through the final slit E and the differential pumping speed to be optimized for each experiment. Close tolerances on the diameter of the tube and the mounting collar F allow this adjustment to be made without disturbing the alignment. Not shown in this figure are the Hastings gauge used to monitor the source pressure and a valved pump-out port which allows the gas supply tube to be pumped out directly instead of through the multichannel slit. These items can be seen mounted on the flange Z in Fig. 5. All parts of the source except for the glass capillary array

* Available from Permeonics Corp., Southbridge, Mass.

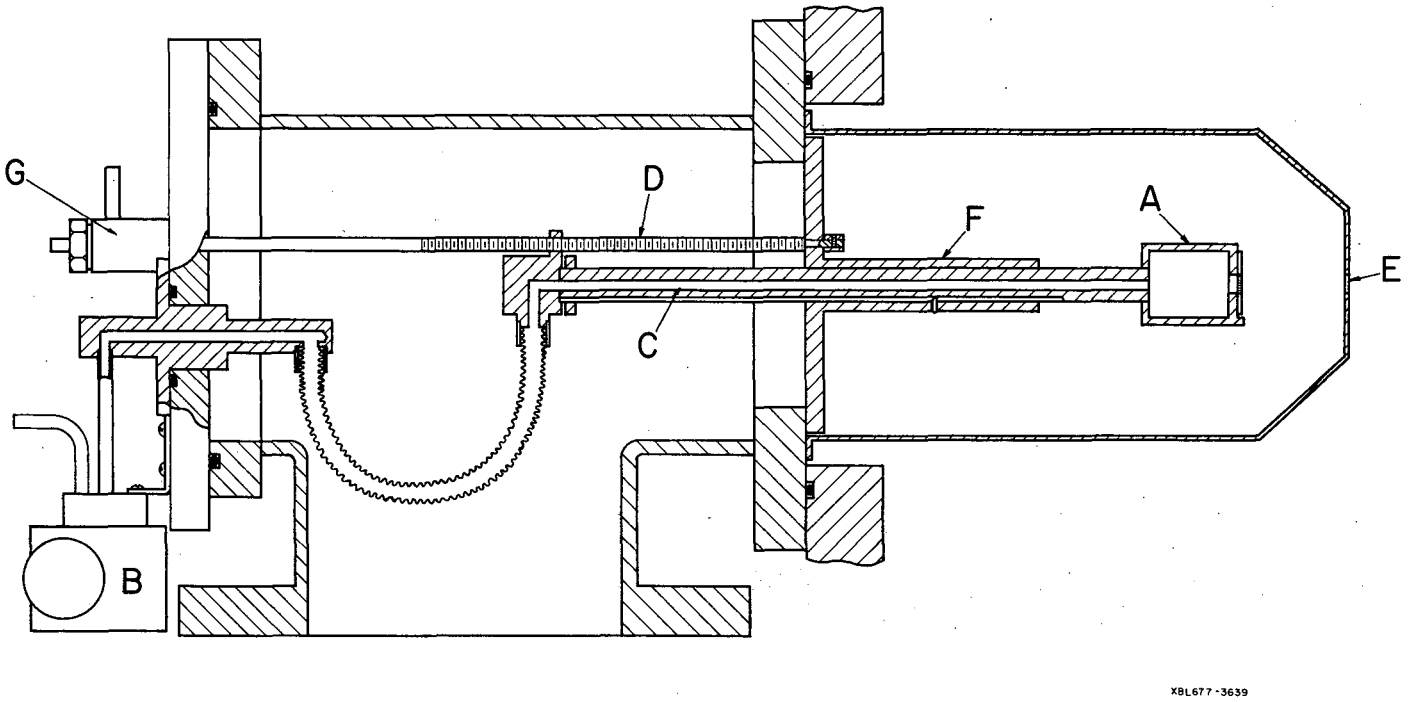

Fig. 15. Multichannel beam source. Shown mounted in main chamber tee. A-Source chamber, B-Variable leak valve, C-Gas inlet tube, D-Adjustment screw, E-Final collimating slit, F-Mounting collar, G-Wilson vacuum seal

are made of Type 304 stainless steel. The screw and mounting collar are lubricated with molybdenum disulfide to prevent spontaneous vacuum welding of the surfaces, to which stainless steel is especially prone.

In tests using N_2, a beam pressure at the crossing point of about 10^{-5} torr was obtained, with 4° FWHM angular divergence and a background pressure of 10^{-6} torr. This rather poor beam to background pressure ratio can be greatly improved, however, by the use of an additional pump mounted in the main chamber face opposite the source to differentially pump the neutral beam after it crosses the ion beam, as shown in Fig. 16.

4. Nozzle Beam Source for Permanent Gases

A nozzle source for permanent gas beams is currently being constructed by Chi-wing Tsao in this Laboratory. The source, which employs two skimmers and has three differential pumping chambers, will couple to the main chamber at face B in Fig. 6. The pump in the main chamber tee will be used to differentially pump the beam through a cone similar to that shown in Fig. 16 with the multichannel source. Provision has been made for modulation of the beam for use with coincidence detection techniques.

5. Neutral Beam Monitors and Detectors

The alkali metal beam intensities were measured with simple hot wire surface ionization detectors similar to those used by all experimenters with alkali metal crossed beams. One of these detectors was mounted permanently in the path of the beam as shown in Fig. 20, and was used to monitor the centerline beam intensity. Another detector was mounted in the rotatable lid and was used to measure the angular distribution of the beam. The detectors consisted of a heated 0.003" diameter tungsten wire suspended vertically behind a slit in the shield and biased at 25V with respect to the ion collector can. This potential proved sufficient

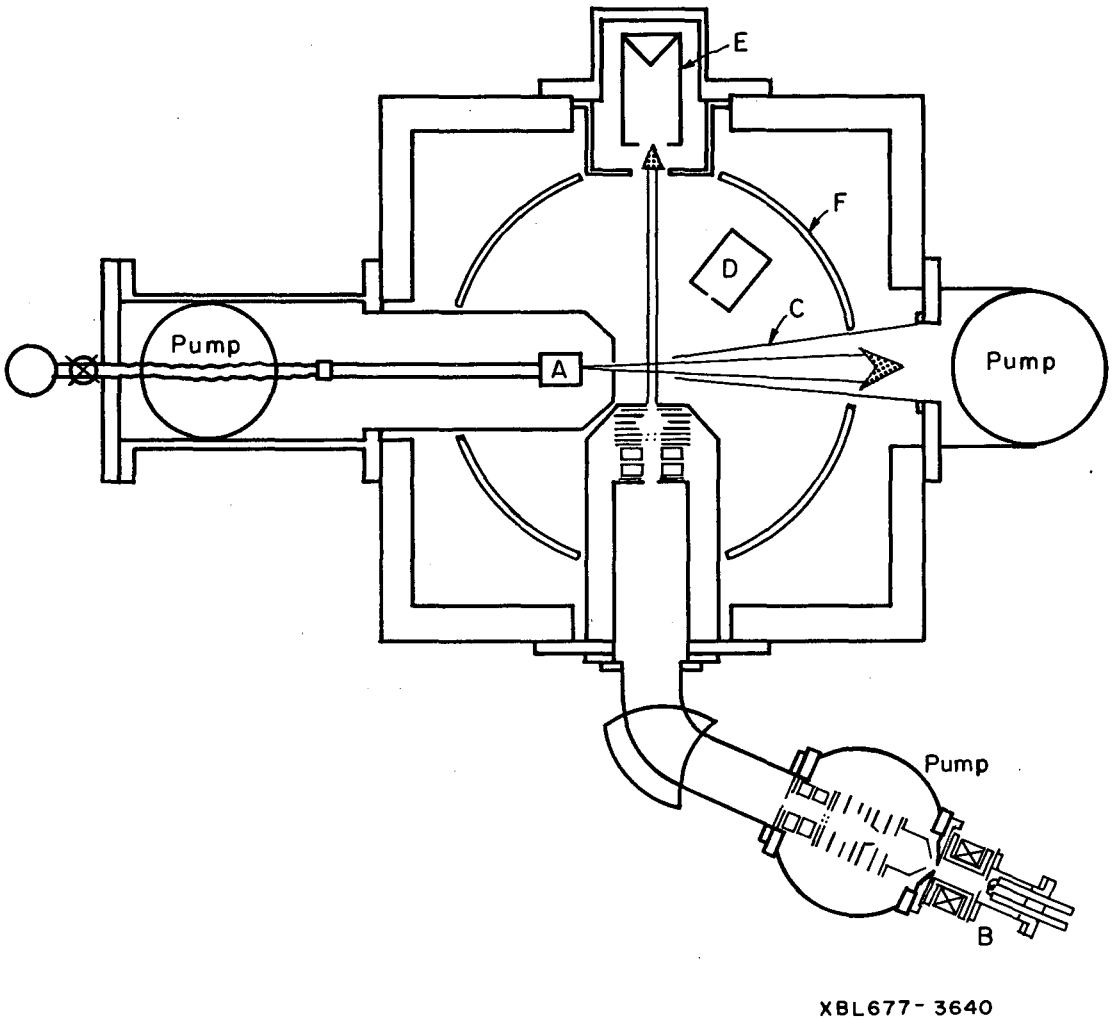

Fig. 16. Schematic diagram of crossed beam experiment with multichannel beam source. Shows proposed differential pumping of the neutral beam after crossing the ion beam path.
A-Multichannel beam source, B-Ion beam source,
C-Differential pumping cone for neutral beam,
D-Detector, E-Ion beam monitor Faraday cup,
F-Copper cold shield

to insure that all of the ions were collected. The ion collector can surrounded the hot wire and was constructed with long channels at the front and rear to allow the beam to pass through but to prevent the escape of ions. Atoms passing through the slit of the detector and not striking the wire passed through the rear of the detector without hitting either the collector or the shield. The dimensions of this detector, which are important in the analysis of absolute cross section data are given in Fig. 21.

For measuring the beam distribution from the multichannel source a detector was used which consisted simply of a 1/2" stainless steel tube connected to an ion gauge, with a 1x2mm slit in the side for the beam to enter. The detector could be rotated with the chamber lid or adjusted vertically, and had a time constant sufficiently short (about 2 sec) to allow the intensity distributions to be measured. For absolute measurements, this detector must be calibrated for each gas with a collimated beam of known intensity, such as can be obtained from a simple effusion source with a thin circular slit.

D. Product Ion Analysis System

The product ion detection system for measurement of differential cross sections consists of an electrostatic energy analyzer followed by a RF quadrupole mass spectrometer and a semiconductor ion counter. Cylindrical electrostatic lenses are used to focus the ions between one component and the next. The detector mounts in one of the rotating lid ports and therefore rotates in the plane of the ion and neutral beams when the previously described sources are used. The electrostatic energy analyzer is a spherical section instrument which bends the product ion beam through 90°, allowing the detection system components to be oriented

vertically. The arrangement is shown in Fig. 17. The analysis components are discussed individually in this section; the next section is devoted to the ion counter.

1. Spherical Electrostatic Energy Analyzer

Electrostatic energy analyzers operate on the principle that the trajectory of a singly charged particle through a static electric field is determined only by its translational energy and is not dependent on its mass. Three field geometries have been rather extensively used to give dispersion between particles of different energy: the homogeneous field between parallel charged plates, and the radial fields between either two cylindrical or spherical surfaces of different potential. The first two geometries give focusing in only one direction. The bi-directional focusing obtained with the spherical electrode arrangement makes it ideal for our purposes.

Two 60°×90° segments are used, with radii of 1.000±0.0003" for the convex surface A and 1.250±0.0005" for the concave surface B. The electrodes are made of Type 304 stainless steel and are gold-plated. They are mounted on precision ground and polished sapphire balls* of 1/8" diameter, which provide electrical insulation and maintain very accurate alignment of the elements. Gold mesh grids of C of 80% transmission serve to attenuate the fringing field at each end of the ion path. Circular apertures are used for the entrance and exit slits D and E. The experimental angular resolution depends on the entrance slit diameter, while the energy resolution depends on the diameters of both the slits. These may be varied according to the requirements of

* Available from Adolf Mellor Co., Providence, Rhode Island.

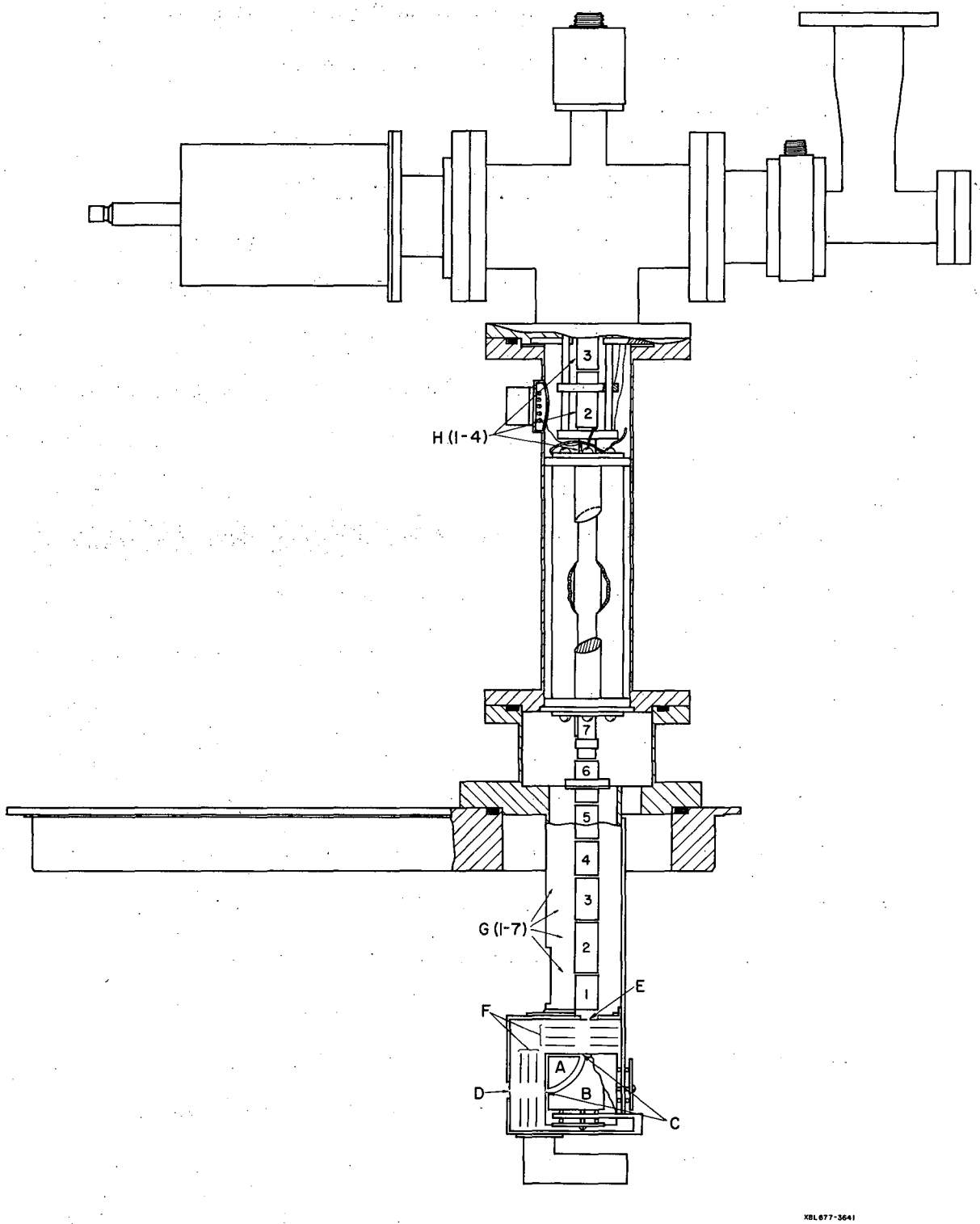

Fig. 17.

Fig. 17 Vertical section of product ion detection system

A Spherical energy analyzer convex element

B Spherical energy analyzer concave element

C Energy analyzer field attenuation grids

D Entrance aperture

E Exit aperture

F Accel-decel electrodes

G First detection system focusing stage

H Second detection system focusing stage

the particular experiment. In all experiments to date, a 1.5mm diameter entrance slit and 2mm diameter exit slit have been used. The energy resolution of the analyzer with these slits is 3% FWHM of the energy for which the analyzer is set. The potential V_{EA} between elements A and B necessary to cause the analyzer to pass singly charged ions of energy E is given by

$$V_{EA} = 0.44\ E \qquad (12)$$

This relation was determined by comparison with retarding potential measurements of the ion energy, and by the dependence of the peak current energy analyzer potential on the ion source potential. The elements are operated with symmetric potentials; i.e., the absolute values of the voltages on A and B with respect to ground are equal. The energy analyzer potential V_{EA} is measured with a John Fluke Model 825 AR/AG differential voltmeter.

The plates F are provided so that the angular distribution of ions may be determined independently of the energy distribution in an experiment where sufficient intensity to do both is not available. In this case, the ions are accelerated between the entrance slit and the first grid to such a high energy that the spread in ion energies is less than the transmission band of the analyzer, thus causing all of the ions to be transmitted. The apertures in F are then used to focus the ions between the slits and the analyzer elements. In ordinary operation they are grounded.

The transmission of the energy analyzer, determined by the two 80% transmission grids, is about 64%.

2. First Detection System Focusing Stage

The ions in the quadrupole mass filter have a transverse component of velocity due to the acceleration of the RF field, and an axial component dependent on the DC potential at which the quadrupole is floated. In order for ions of different mass to be separated, the latter velocity must be low enough to allow the ions to make many oscillations while traveling through the mass spectrometer. This means that the ions emerging from the energy analyzer at any energy must be focused into the mass filter at the same low energy (about 15 eV). To do this the cylindrical lens elements G(1-7) are used. In tests to determine the optimum focusing mode, it was found necessary only to vary the potentials of elements 2, 6 and 7, leaving the others grounded.

To determine the optimum focusing voltages as a function of ion energy, the product ions from the reactions of N_2^+ with H_2, D_2 and CH_4 have been used. Setting the floating potential of the quadrupole such that the DC level of the ions in the mass filter is 15 eV, the potentials of these three elements are varied to give the maximum current at the ion counter. After the optimum focusing voltages are determined at a series of energies in the range desired, computer interpolations of the voltages are used to generate a table of focusing potentials versus energy analyzer settings. These voltages are then translated into helipot dial settings so that it takes only a few seconds to adjust the focusing voltages to the optimum values for any energy analyzer potential. Using the primary ion beam for comparison of the current emerging from the energy analyzer with the current reaching the detector, it was found that with our tabulated focusing conditions the transmission of the detector system after the energy analyzer

(including the quadrupole mass filter) is constant as a function of energy and equal to about 50%.

3. Quadrupole Mass Spectrometer

Our quadrupole mass filter and power supply are virtually identical to those described by Kent Wilson and Marvin Hartley.[13] The only important modifications were that provision was made for floating the quadrupole at a DC level up to several hundred volts, and that the RF rectifier was removed from the main chassis and mounted on the rotating lid of the main chamber so that the cables to the quadrupole, which are part of the RF tuning circuit, could be made short.

For experiments in which mass analysis is not required the quadrupole mass filter section of the detection system may be removed, and the ion counter mounted directly above the energy analyzer.

4. Second Detection System Focusing Stage

To extract the ions from the mass filter and focus them on the electron emission surface of the ion counter, the cylindrical elements H(1-4) are used. Because the ions are to be accelerated to much higher energies than the initial energy of the ions, it is unnecessary to adjust the potentials on these elements when the energy analyzer setting if varied. The potentials used are -3000V on elements 2 and 4 and -700V on elements 1 and 3. These values are not critical.

E. Ion Counter

1. General

As noted in Chapter I, the ultimate possible sensitivity in the detection of product ions is obtained when the ions are counted individually. Successful ion counters have been built which utilize the

Fig. 18 Cutaway drawing of ion counter

H Second dectection system focusing stage

I Electron emission surface

J High voltage lead

K Lithium-drifted silicon semiconductor

L Anti-corona ball

M Wilson vacuum seal

N Field effect transistor

O Flange to mount liquid nitrogen reservoir

P Boron nitride mounts

Q Electrical feedthrough ring

R Faraday cup

pulse of electrons emitted when the ion impacts at high energy on a metal surface--either by multiplying the initial electron pulse through subsequent dynode stages, as in an electron multiplier,[24] or by allowing the electrons to impinge on a scintillator, the emission of which is monitored by a photomultiplier tube.[25,26] Although counters of high efficiency and stability have been reported employing both of these techniques (particularly the scintillation method), the recent advances in technology and instrumentation for semiconductor radiation detectors made at the Lawrence Radiation Laboratory induced us to construct a new detector which adapts a semiconductor counter originally designed for nuclear spectrometry to the detection of slow positive ions. The resultant counter, which we believe to be unexcelled in efficiency, stability and ease of operation, is shown in relation to the other detection system components in Fig. 17, and in detail in Fig. 18. It can be used for ion currents in the range from well below one ion per second to over 10^5 ions per second.

The principle on which the counting system operates is straightforward. As the ions emerge at 3 KeV from the focusing system H, they are drawn to the electron emission surface I by a high negative acceleration potential E_a (usually about 25 to 30 KeV) applied through the high voltage lead J. An ion striking the surface emits an almost instantaneous pulse of electrons. Each of these is accelerated by the potential of the emission surface across the gap into a silicon wafer K, which is covered with a thin coating of gold used to bias the front face at -300V. A pulse containing n electrons, then, acquires an energy of approximately nE_a. Except for a small amount absorbed in the gold layer, this energy is entirely dissipated in collisions within the wafer, which

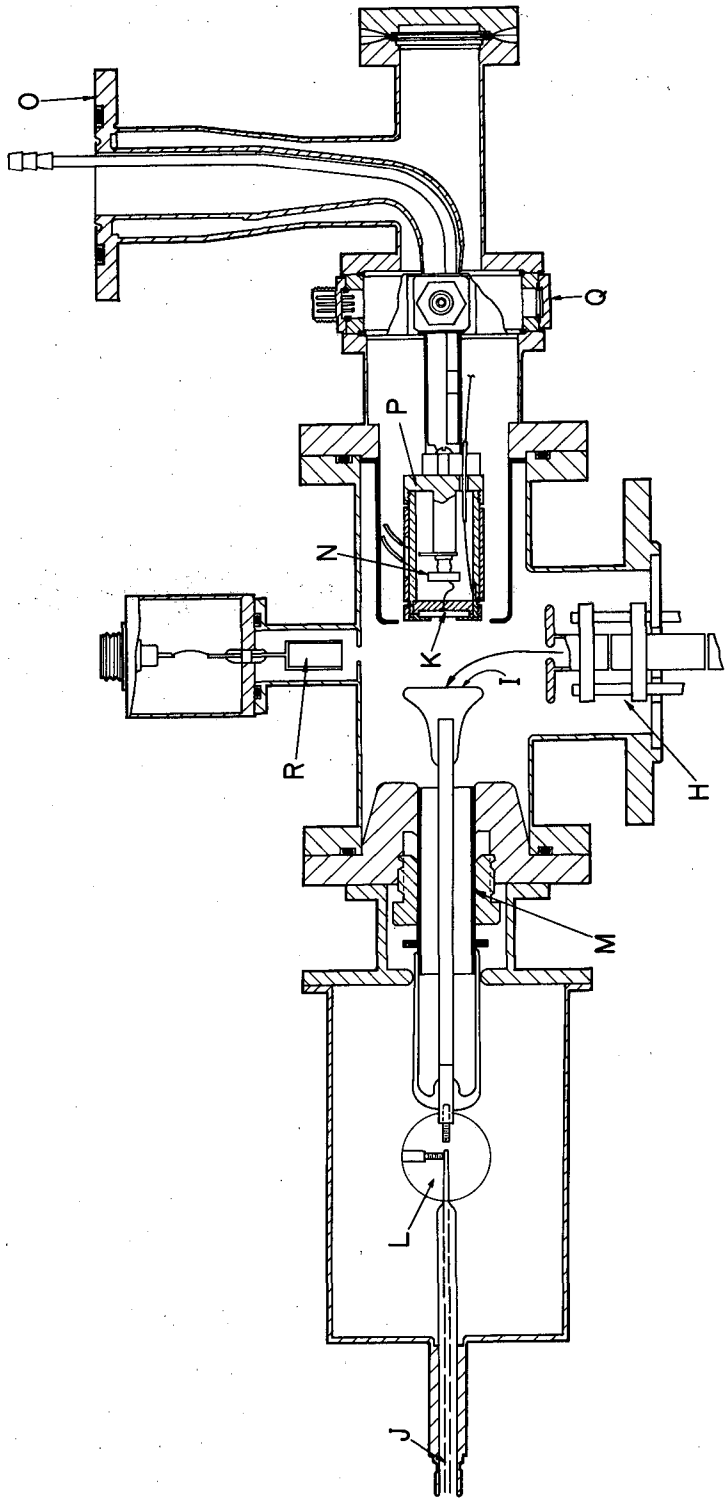

Fig. 18.

excite a large number of silicon valence electrons into the conduction band, causing a current to flow between the front and back faces of the semiconductor. The current pulse is picked up by a field effect transistor (FET) preamplifier and fed into a linear amplifier system which drives the scaler.

2. Construction

The cathode surface I is a layer of aluminum of about 1000Å thickness evaporatively coated on a highly polished stainless steel surface. Aluminum was chosen because of its high electron emission from ion impact. An anti-corona ball L is used to connect the high voltage lead to the emitter, which is electrically insulated by the glass envelope vacuum seal. The emitter assembly is mounted in a Wilson seal M. By varying the position of the cathode, the ion focusing may be adjusted to cause the beam to strike the center of the surface I. This adjustment is not critical. The edges of all metal pieces in the vicinity of the cathode are rounded and polished to minimize field emission.

The components principally responsible for the performance of the detector are the semiconductor and the FET preamplifier, both of which are manufactured at LRL. The construction and operating characteristics of these items have been described in detail by Goulding,[27] and only a superficial description will be included here.

The semiconductor is a 3mm thick piece of p-type silicon in which the impurities have been well compensated by drifting with lithium atoms. By this method a region where conduction is intrinsic (due mostly to the promotion of silicon valence electrons into the conduction band) is obtained which extends through the entire crystal. This makes the leakage current through the material very low under equilibrium con-

ditions, especially at low temperatures--consequently making the charge pairs produced by electron impact more easily detectable. The exposed area of the detector is a 1 cm diameter circle. A potential of 300V between the front and back faces of the crystal is used to sweep out the current pulse. Obviously, the highest mobility of the electrons and holes is desired in order to produce a sharp pulse; therefore the semiconductor is operated at liquid nitrogen temperature, where the mobilities of both electrons and holes are about a factor of 40 greater than the respective mobilities at room temperature. A short lead connects the copper contact on the back of the semiconductor to the field effect transistor N, which also is operated at liquid nitrogen temperature to minimize noise. The rest of the preamplifier is mounted outside the vacuum system (see Fig. 4). Liquid nitrogen is supplied from a reservoir mounted on flange O. The detector mounts P are machined from a boron nitride block, which provides good electrical insulation and thermal conduction. The other ion counter parts are made of type 304 stainless steel or of aluminum alloy. Vacuum feedthroughs mounted in the ring Q are used to make the bias voltage and preamplifier connections. The Faraday cup R can be used when the cathode voltage is turned off to monitor the ion current.

3. Instrumentation

The linear amplifier system used with the ion counter was developed and built at LRL* and has been described by Goulding and Landis.[28] The system uses all solid state components and is mounted on a single 7" panel. The pulse amplifier, which has excellent linearity over the

* Identical components are now available from Technical Measurements Corp., New Haven, Conn.

output range 0.2 to 8V, will accept pulses of positive or negative polarity, has variable gain, and includes a pulse shaping network with variable time constant. The natural rise time of the amplifier is only 80 nanoseconds. Other components included in the system are a single channel analyzer with upper and lower cutoffs independently adjustable, a biased amplifier, and both fast and slow coincidence circuits. Interconnection between these units are made on the back of the chassis. Our counting equipment includes a Model NS-11 timer, two Model NT-16 10MC scalers and a Model NR-10 linear ratemeter from Hamner Corp. A Hamner Model NE-11 scanner is used to translate the timer and scaler digital outputs and feed them to a Model 33 TC Teletypewriter which simultaneously prints the data and punches it on paper tape.

A Kilovolt Corp. Model KVR 50-5 power supply with an output of up to 50 KV is used to power the cathode. This unit was selected because of its low (0.01%) ripple to avoid pickup problems on the field effect transistor.

4. Operation

For pulse height analysis, the output from the linear amplifier is fed, after pulse shaping, to a 400 channel pulse height analyzer through the biased amplifier. For ordinary single channel counting, however, the linear amplifier output is simply connected to the single channel analyzer, which puts out a constant amplitude (~ +4V) pulse to drive the scaler, and whose lower level is set to attenuate all noise pulses, but to let through a pulse equivalent in energy to 1 electron striking the detector.

Obviously, one must know how to set the cutoff level. For this purpose the preamplifier is provided with a test pulse input, which can be used for calibration of the discriminator. It was found by matching the output pulse heights that a 15 mV amplitude test pulse into the preamplifier is equivalent to the 122 KeV pulse obtained by irradiating the detector with gamma rays from Co^{57}. After one adjusts the linear amplifier gain so that a one electron pulse in the semiconductor gives an output pulse at least equal to the 200mV system minimum, the discriminator may be set by feeding in a test pulse of amplitude corresponding to the desired cutoff energy and turning up the discriminator level until the output pulses are just attenuated. The cutoff level and amplifier gain do not drift significantly over long periods of time; therefore this adjustment need be made only once unless the electron energy E_a is changed or unless one desires to cut off the pulses at a different relative energy. After the discriminator has been set, the day to day operation of the detector in this mode is extremely simple: fifteen minutes after the liquid nitrogen is added to the reservoir the detector is cool; the linear amplifier system and the semiconductor bias and cathode potentials are then turned on and the detector is ready to count all incident ions.

Future plans include the use of coincidence counting techniques to eliminate background signals when the ion beam is crossed with a modulated neutral beam. The only additional equipment needed is a phase shifter to go between the reference frequency source and the external coincidence input of the linear amplifier system. In this mode the phase shift will be adjusted to give the maximum difference between the coincidence and anticoincidence signals, under which condition one

scaler will count all of the pulses striking the detector while the other will register only background counts.

5. Resolution and Efficiency

The number of electron-hole pairs created in the semiconductor is proportional, within a statistical fluctuation of course, to the energy of the input pulse and hence to the number of electrons in the input pulse, since each has the same energy. The principle advantage our detector has over the electron multiplier and scintillation types is its ability to resolve pulses containing different numbers of electrons on the basis of the corresponding output pulse heights. In an electron multiplier, this information is lost through averaging over all the dynode stages. Though the average output pulse height from the scintillation counter is roughly proportional to the energy of the pulse striking the scintillator, the inefficiency of the scintillation and photoemission mechanisms requires that the average energy expended to produce a photoelectron be very high, resulting in large statistical fluctuations in the pulse heights.[29] In our detector, on the other hand, a hole-electron pair is produced for an average energy of 3 eV dissipated in the semiconductor (typically a factor of 100 less than the average energy required by a scintillation detector for the emission of one photoelectron[29]). Thus at the normal acceleration voltages used about 10^3 charge pairs are produced for every electron striking the detector. This results in a rms fluctuation of only 3% if normal statistics is obeyed in the excitation process. In fact, however, due to the high (about 30%) yield in the fraction of the total energy used for ionization, normal statistics is not obeyed, and recent experiments indicate that the actual signal spread may be only about half of this amount.[30]

Under operating conditions, subsequent spreading in the electronics due to the background noise reduces the resolution to an optimum value of about 3 KeV FWHM, which is more than adequate for our purposes.

A typical pulse height distribution measured with our detector and a 400 channel pulse height analyzer for approximately 25 KeV N_2^+ colliding at 45° with the aluminum emission surface is shown in Fig. 19. The peaks are resolved out to about n = 14.

In the absence of quantitative data, a Poisson distribution

$$P_n = e^{-\alpha} \frac{\alpha^n}{n!} \qquad (13)$$

where α is the average number of electrons in the pulse, has generally been assumed for the number n of electrons emitted when a heavy ion impacts at high energy on a metal surface.[24,26] With our detector it is possible to test this assumption. The Poisson distribution with $\alpha = 6$ chosen to match the experimental peak is plotted (open circles) in Fig. 19. There appears to be a significant difference between the two distributions, the experimental probabilities being relatively greater for both high and low n. Similar results have been found for other N_2^+ energies, indicating that normal statistics may not govern the electron emission. This appears to be an interesting and fruitful area for further study.

The greatly improved pulse energy resolution of this detector over that of the other types has important implications concerning both efficiency and the discrimination against noise pulses. The efficiency of any ion counter may be thought of as the probability that the particle will generate the initial pulse times the probability that the pulse will remain detectable through all subsequent amplification stages. For our

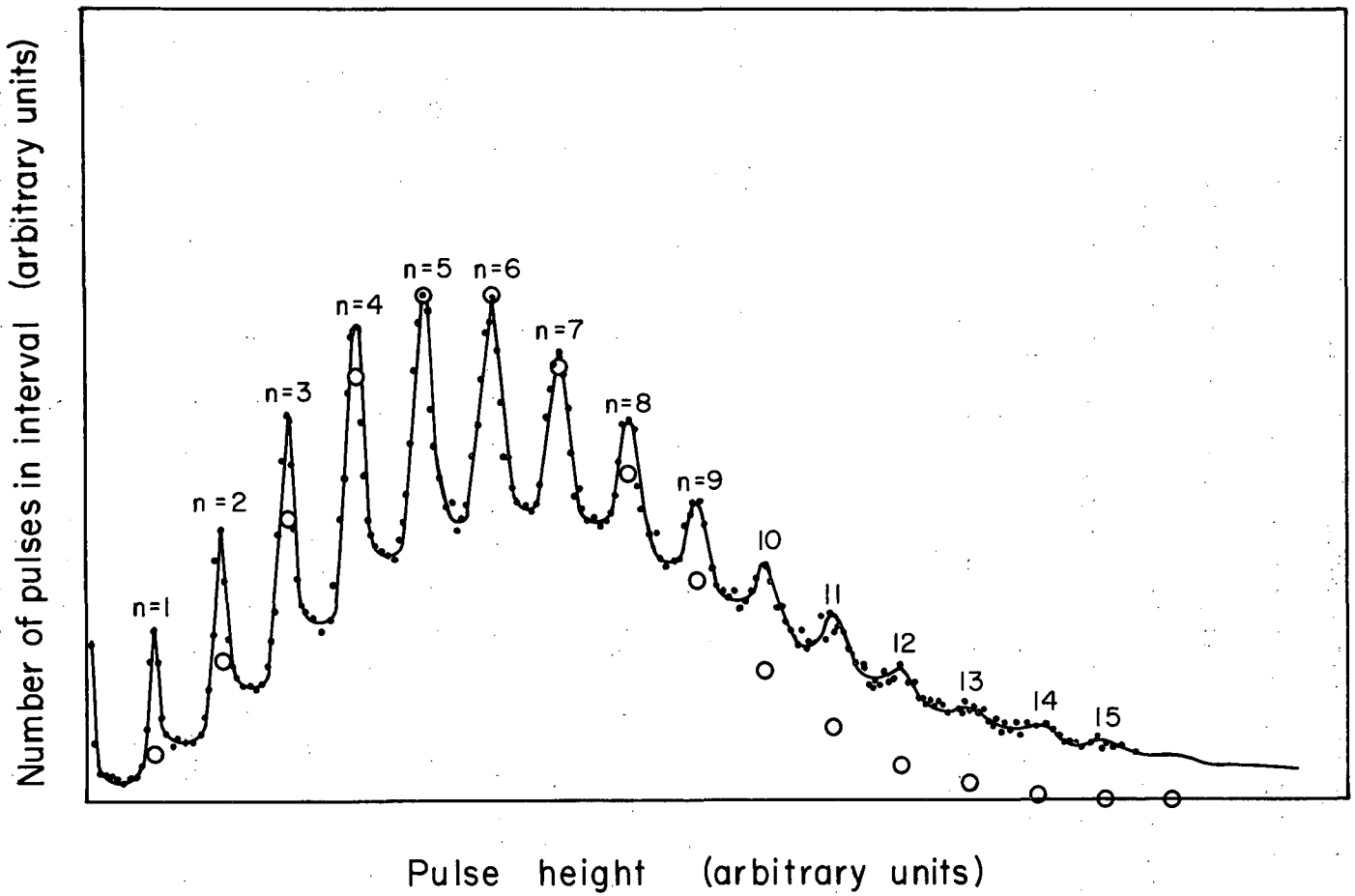

Fig. 19. Detector pulse height distribution for 25 keV N_2^+ ions, showing resolved peaks corresponding to integer numbers of electrons in the emission pulse. Open circles represent a calculated Poisson distribution with $\alpha = 6$.

counter, as well as for the others mentioned above, the first factor in the efficiency is the probability of at least one electron's being emitted when the ion strikes the emitter surface. Because the focusing in our detector insures that every electron emitted by the surface I will be propelled into the silicon wafer, and because the high single-stage gain of the semiconductor-preamplifier network gives a probability of essentially unity for the detection of each electron, the efficiency of our detector is governed by the electron emission factor alone. In the electron multiplier, on the other hand, there may be a significant probability that a single electron emitted in the first stage will not be detected due to the low gain of the next stage (which, for example, will be only 2 for a 20-stage electron multiplier with an overall gain of 10^6). The scintillation counter also typically suffers small losses, due to imperfect collection of the light emitted by the scintillator. A pulse height discriminator must be used in the scintillation counter to discriminate against the high intensity low amplitude pulses from the photomultiplier dark current. Because of the poor resolution, however, it is necessary to set the cutoff limit so high that part of the signal is also attenuated in order to obtain an acceptable background level. The noise level in our detector, by contrast, is sufficiently well resolved from the n = 1 peak that the discriminator may be set to allow all single electron pulses to be counted while maintaining a background counting rate of only 20 cpm. The background may be reduced to less than 10 cpm with only a small loss in sensitivity if the discriminator is set to cut off the n = 1 and n = 2 pulses.

6. Stability

Semiconductor detectors used for nuclear research are damaged by high energy fission fragments and to a lesser extent by neutrons, gamma rays, and high energy (> 250 KeV) electrons.[31] Since our semiconductor is bombarded only with electrons of much too low an energy to displace an atom from the lattice, no deterioriation in the performance of the counter is anticipated. In the seven months the detector has been in use, no maintenance of any kind has been required.

CHAPTER IV

Operation and Data Analysis

This section describes the operation of the apparatus in the two modes which have been used thus far to obtain new information on ion-neutral interactions. The discussion is intended to provide an illustration of the practical details which must be considered in doing beam experiments with this apparatus, as well as to give an explicit account of our experimental procedure and data analysis for those who are interested specifically in the results of these investigations.

A. Measurement of the Total Absolute Resonant Charge Transfer Cross Sections for Cs^+-Cs, Rb^+-Rb, and K^+-K in the 10-500eV Energy Range

Since the resonant transfer of electrons between atoms can occur over rather larger distances than the atomic diameters, most of the collisions resulting in charge transfer have sufficiently large impact parameters that the particles are deflected only very slightly from their original trajectories. Thus, in a crossed beam experiment most of the ions created by charge transfer will be found traveling in the direction of the neutral beam, with the original velocity of the atoms (which is much smaller than that of the ions). The cross section may then be determined by measuring either the number of slow ions appearing in the neutral beam or the number of ions missing from the ion beam.

1. Experimental Arrangement and Instrumentation

A schematic of the apparatus set up for the alkali metal experiments is shown in Fig. 20. Ions were drawn from the surface ionization source A with a relative potential of -500V on the extractor cone B and were focused into the mass spectrometer chamber (which is grounded) with a series of cylindrical lenses C. The momentum analyzed beam was collimated by an einzel lens D just before crossing the neutral beam. The momentum spread of the final ion beam was 1.5% FWHM at energies above 50 eV and increased to 2% at 10 eV. The angular spread of the ion beam was about 2° FWHM.

The nozzle source for neutral beams E was mounted as described previously, and the collimating slit adjusted to give a beam of 5° FWHM angular divergence. The hot wire surface ionization detector F was used to monitor the neutral beam centerline intensity and a similar detector (not shown) was mounted on the rotating lid and used to measure the angular distribution. In several experiments the vertical distribution of the neutral beam was measured and the intensity found to be uniform to within about 1% over the distance intersected by the ion beam.

For measurements both of the attenuation of the ion beam and of the slow ion current a Faraday cup detector G was used which could be rotated into either position desired. The cup was surrounded by a shield with a 1" diameter aperture adjusted to a distance of 1.072" from the beam crossing point. Thus, the acceptance angle of the cup was ±25° from the scattering center. This detector was used with a Keithley Model 417 High-Speed Picoammeter and Moseley 2D-2A X-Y recorder. The electrometer-recorder combination was calibrated versus a Keithley picoampere source with an overall accuracy of ±0.4% on the ranges used in these experiments.

Fig. 20 Schematic diagram of the apparatus set up for measurement of alkali metal charge transfer cross sections

A Ion beam source

B Extractor

C Cylindrical focusing lenses

D Einzel lens

E Nozzle beam source

F Neutral beam monitor

G Ion collection Faraday cup

H Ion beam monitor Faraday cup

I Neutral beam flag

J Cold slit

K Hot collimating slit

L Charged particle deflection electrodes

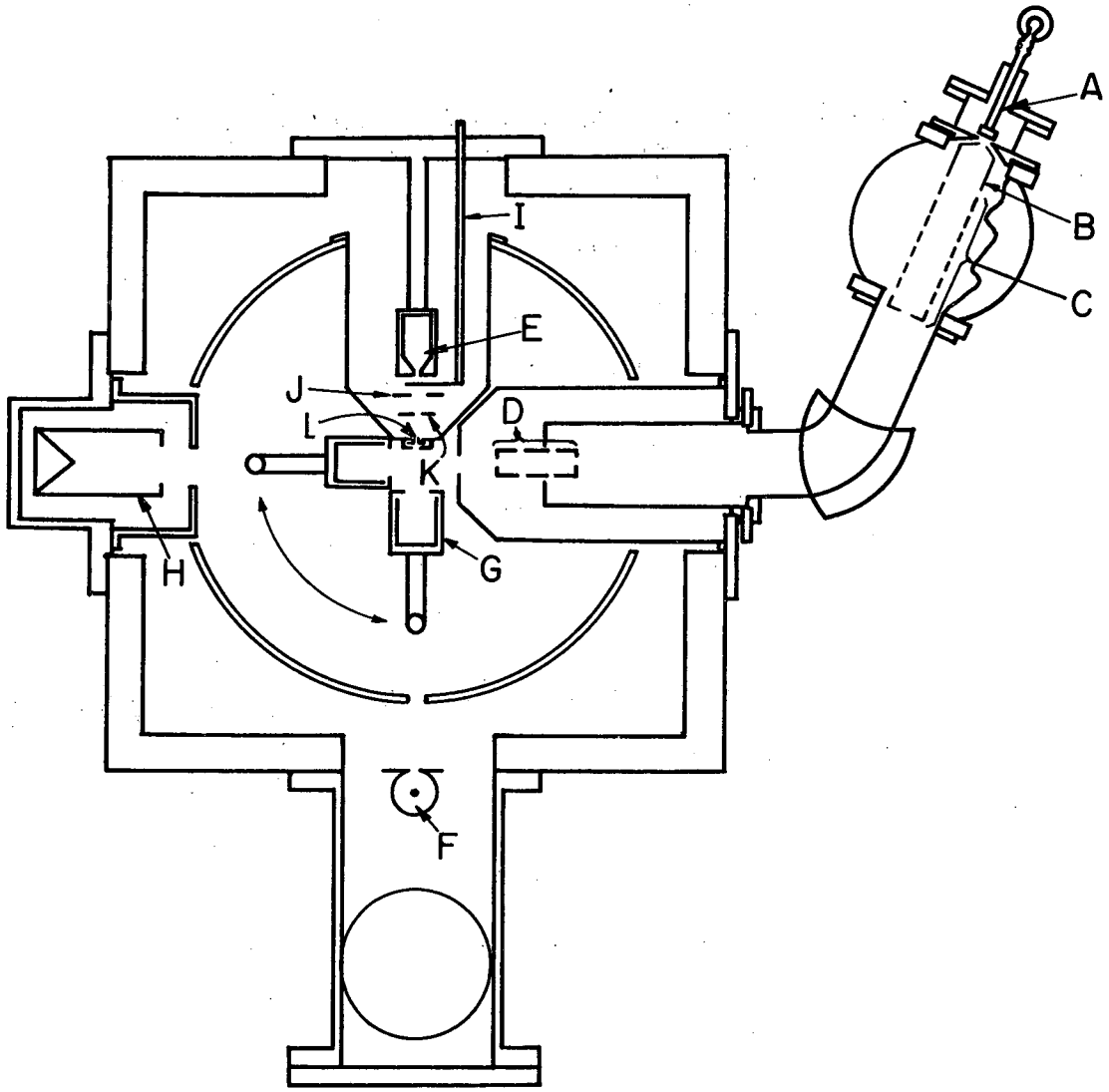

Fig. 20.

A Cary Model 31 vibrating reed electrometer with remote input head was used to monitor the ion beam current on the Faraday cup H and to measure the neutral beam distribution. The input resistors used in these experiments were measured to ±0.1%. The neutral beam intensity was monitored with a Keithley Model 610B electrometer. Since only relative values on the same range were required, this electrometer was not calibrated.

2. Procedure

General

In preparation for each day's experiments, the neutral beam oven, the cold shield surrounding the oven, and the Faraday cup detector were removed from the chamber, washed in dilute acid and distilled water to remove the alkali metal accumulated in the previous experiment, rinsed in absolute methanol and dried. The large cold shield was washed with distilled water and methanol through the port of the chamber. After reinstalling the detectors and cold shield and checking the alignment of all components, the recharged neutral beam source was quickly installed and the system pumped down immediately. After a pressure of less than 10^{-6} torr was achieved, the liquid nitrogen reservoir was filled and the cold shield allowed to cool overnight.

It was generally found that the longer the ion beam was operated at a given energy the more stable it became, and that it was easier to produce stable beams of high intensity if the experiments were done with monotonically increasing ion energy. Therefore, about an hour before the measurements were to begin, the ion beam source was turned on and the operating conditions adjusted to produce a beam at the lowest energy to be used that day. After the ion beam had become stable, the neutral

beam was produced. By heating the oven rapidly at first, then decreasing the power to just the amount necessary to maintain the oven at the desired temperature, it was possible to produce a stable beam of the desired intensity in about 1/2 hour. The temperature of the neutral beam oven was recorded continuously throughout the experiment. The approximate oven temperatures used and corresponding vapor pressures for the three metals were

K --- 665°K, 3.5 torr

Rb --- 610°K, 3 torr

Cs --- 585°K, 2.5 torr.

Measurements of both the attenuation of the primary ion beam and the slow ion current in the neutral beam direction were made for cesium and rubidium, but because of the low cross section only the slow ion collection method was used for potassium. When both sets of experiments were done on the same day it was necessary to do the attenuation measurements first, because the surface ionization of metal deposited on the Faraday cup during the slow ion collection caused a prohibitively high background current when the cup was unbiased.

Attenuation Method

In measurements of the ion beam attenuation the Faraday cup was positioned exactly opposite the ion beam source exit slit, so that the ion beam passed into the center of the detector aperture. The ion beam energy was set at the desired value and the focusing conditions adjusted to give the maximum intensity and stability (subject to time limitations). The bulk of the ion current was then biased out and the electrometer sensitivity increased so that the attenuation would be a large fraction of the full scale current. Since the attenuation was usually of the

order of 1%, this necessitated a 10- to 100-fold increase in sensitivity. With the X-axis of the recorder on a time scale of 10 sec/in., the electrometer output was then recorded as the neutral beam flag was opened and closed at intervals of several seconds. When the number of cycles was deemed adequate for accurate measurement, the electrometer bias current was quickly turned off and the total ion current read and recorded. From extrapolation of the line of drift of the ion current to the time at which it was measured, the total ion current for any point on the trace was known. For each trace the ion energy, the neutral beam monitor current, the electrometer ranges used in measuring the total ion current and the attenuation, and the recorder range were recorded. The background current due purely to the neutral beam was measured by shutting off the ion beam and recording the current to the Faraday cup detector as the neutral beam flag was opened and closed as before. This background current was subtracted from all the signals. The neutral beam monitor was turned off during all the measurements of both the attenuation and slow ion current, and the charged particle deflection plates at the neutral beam exit slit were adjusted to minimize the background, which was only a small fraction of even the lowest signals measured.

Two methods were employed to measure the attenuation signals (i.e., difference in the unattenuated and attenuated envelopes) from the recorder traces. Where the electrometer noise and ion beam current drift were low it was found to be simplest to measure the distance between the envelopes at several places in the trace and average them. Where the electrometer noise or the ion beam current drift was large, the most accurate and reproducible method was to trace one of the

envelopes on tracing paper then shift the paper a measured distance such that the traced segments gave the maximum continuity with the other envelope.

Slow Ion Collection Method

To measure the current of slow ions created by charge transfer, the Faraday cup was rotated into the path of the neutral beam and biased through the electrometer head at a potential sufficiently negative to collect all of the slow ions in the vicinity of the scattering center. With low energy ion beams the necessary bias potential (about 6V) was large enough to significantly deflect the primary ion beam; therefore these measurements do not extend to the lowest energies covered in the attenuation experiments.

These experiments were carried out in much the same way as the attenuation measurements, except that the primary ion current was measured with the ion beam monitor cup and that it was unnecessary to apply a bias current to the detector. The total ion current was recorded by hand each time the neutral beam flag was closed. After each trace was made, the Faraday cup was lifted out of the path of the neutral beam and the monitor current was recorded. Also, the ion energy, Faraday cup bias potential and electrometer and recorder ranges were recorded for each trace. The background current due to the neutral beam was measured in the same way as before and subtracted from the signals.

Measurement of the Neutral Beam Distribution

To obtain the angular distribution of the neutral beam the output of the electrometer measuring the neutral beam detector current was connected to the Y-input of the recorder and the X-input was taken

from a battery powered voltage divider (helipot) connected to the sprocket used to rotate the lid of the main chamber. With care taken to avoid backlash in the helipot and recorder, the detector was slowly rotated through the neutral beam as the intensity was recorded. The X-axis was calibrated on each curve by marking the angle at each end of the trace. Before and after each curve was traced the neutral beam monitor current was measured.

Because of early experiences where the shape of the neutral beam distribution changed during the course of a day's experiments due to collection of beam material on the cold slit of the source, the beam flag was kept closed at all times except when actual measurements were being made. In the experiments reported, the distribution was measured several times during the period in which data was being taken in order to insure that the integral of the distribution normalized to the monitor current remained constant.

3. Calculation of the Cross Section

Assuming that the process giving rise to the signal is wholly charge transfer, the cross section is simply

$$\sigma = \frac{F}{\int \rho dx_i} , \qquad (14)$$

where under thin target conditions F is the scattering fraction (signal divided by the total ion current) and $\int \rho dx_i$ is the integral of the neutral beam density ρ over the path x_i of the ion beam. F is easily calculated by correcting the measured signal and ion beam currents for the background and the calibration factors for the electrometers. The quantity $\int \rho dx_i$ can be calculated from the integral of the neutral beam

intensity distribution in terms of the detector dimensions shown in Fig. 21 and the following parameters:

n = number of particles per unit time striking the detector wire

e = charge on each ion collected

ϵ = ionization efficiency of wire

$\phi_o(x_i)$ = flux of neutral beam particles along the ion path

s = distance along the path of the detector

A = area under the neutral beam intensity distribution curve (units of in. Rec. X-in. Rec. Y)

g = ratio of distance along the detector path of distance along the X-axis of the trace

β = ratio of detector current to distance along the recorder Y-axis (units of amp/in. Rec. Y)

γ = ratio of detector angle to distance along the recorder X-axis (units of °/in. Rec. X).

The rate at which particles strike the detector wire is

$$n(s) = \phi_o(x_i)\, c \left(\frac{a}{f+a}\right) d \left(\frac{a}{a+b}\right) \tag{15}$$

and the current measured is

$$i = nee = cdee\left(\frac{a}{f+a}\right)\left(\frac{a}{b+a}\right) \phi_o(x_i) \,. \tag{16}$$

Considering the contribution to the density ρ from the particles in each velocity element dv separately, the density (at a given x_i) is

$$\rho = \int_o^\infty \rho(v)\, dv = \int_o^\infty \frac{\phi(v)}{v}\, dv \,. \tag{17}$$

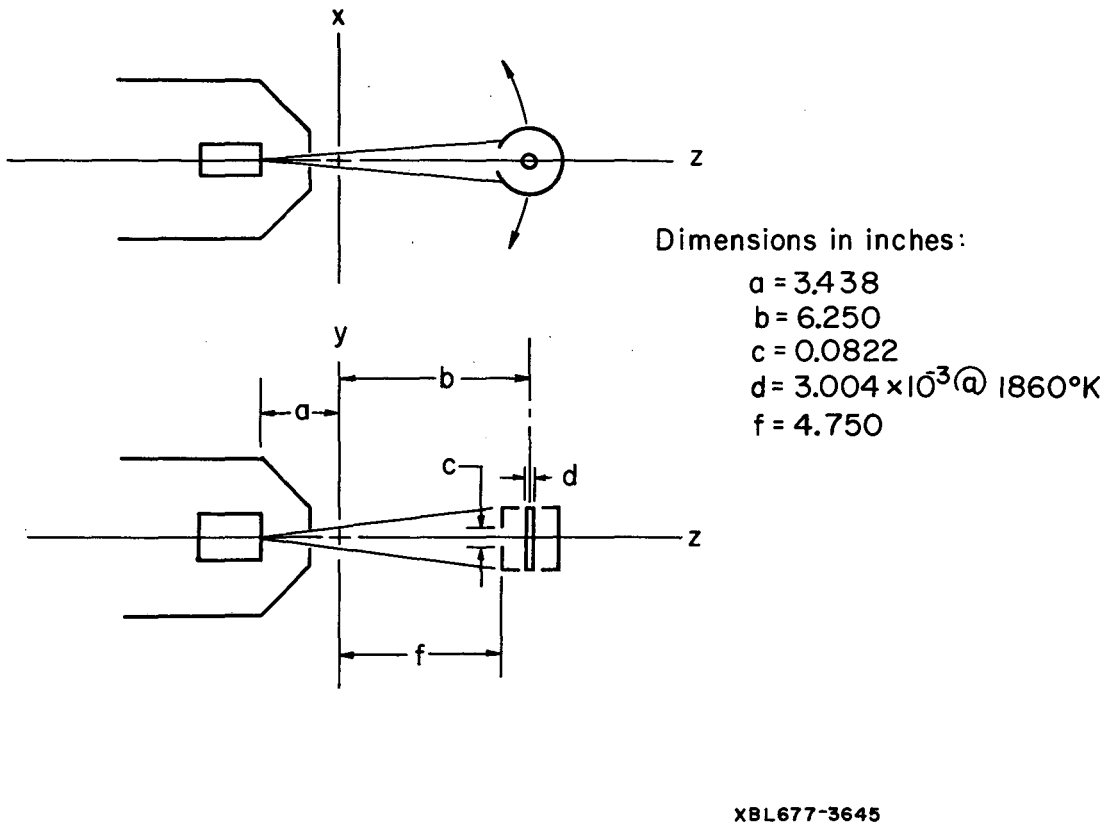

Fig. 21. Alkali metal neutral beam detector geometry.

If the velocity distribution in the beam is Maxwellian, the flux may be written

$$\phi(v) = \frac{2\phi_o}{\alpha^4} v^3 e^{-v^2/\alpha^2} . \tag{18}$$

where $\alpha = (2kT/m)^{1/2}$. Under these conditions, then, the density is

$$\rho = \frac{2\phi_o}{\alpha^4} \int_o^\infty v^2 e^{-v^2/\alpha^2} dv = \frac{\sqrt{\pi}\,\phi_o}{2\alpha} , \tag{19}$$

which may also be written as

$$\rho = \frac{\phi_o}{\bar{v}} \tag{20}$$

Here

$$\bar{v} = \frac{2\alpha}{\sqrt{\pi}} \tag{21}$$

is given by the same expression as the average velocity of the particles in the source, and

$$\phi_o = \int_o^\infty \phi(v)dv = \frac{1}{cde\epsilon} \left(\frac{f+a}{a} \right) \left(\frac{b+a}{a} \right) i \tag{22}$$

from Eq. (16). It is important to note that the average velocity to be used in the calculation of the density from the detector current is <u>not</u> the average velocity of particles striking the detector, $3/4\sqrt{\pi}\,\alpha$, which is obtained by averaging the particle velocities over the distribution in Eq. (18).

Combining Eqs. (22) and (20) we have the expression for the density in terms of the measured current,

$$\rho = \frac{1}{cde\epsilon\bar{v}} \left(\frac{f+a}{a}\right)\left(\frac{b+a}{a}\right) i \quad , \tag{23}$$

which may be integrated over the ion path to give the quantity desired in Eq. (14):

$$\int \rho dx_i = \frac{1}{cde\epsilon\bar{v}} \left(\frac{f+a}{a}\right)\left(\frac{b+a}{a}\right) \int i \, dx_i \quad . \tag{24}$$

The detector, of course, measures the current along the path s instead of the path x_i, and the integral of the distribution curve is related to the current integral by

$$A = \frac{1}{g\beta} \int ids \quad . \tag{25}$$

For beams of small angular divergence, however, the path s may be approximated by the straight line path x_d, where

$$dx_d = \left(\frac{b+a}{a}\right) dx_i \quad . \tag{26}$$

Substituting in the integral and rearranging we have

$$\int i dx_i = \left(\frac{a}{b+a}\right) g\beta A \quad . \tag{27}$$

Also, since γ is easily measured from the trace whereas g is not, it is convenient to make the substitution

$$g = \frac{b\pi\gamma}{180^\circ} \quad . \tag{28}$$

This yields, finally, the expression for the integrated density in terms of measurable parameters and apparatus dimensions:

$$\int \rho dx_i = \frac{(f+a)\, A\beta\gamma b\pi}{180^\circ acde\epsilon \bar{v}} \tag{29}$$

or, if $\bar{v}$ is expressed in cm/sec,

$$\int \rho dx_i = 2.589 \times 10^{21} \left[\frac{A\beta\gamma}{\epsilon\, \bar{v}} \right] . \tag{30}$$

Since the neutral beam intensity changed slightly over the course of the day's experiments, it was necessary to normalize both the scattering fraction F and the integrated density to the neutral beam monitor current recorded for each measurement. The cross sections were actually calculated from

$$\sigma = \frac{F_N}{\int \rho_N dx_i} \tag{31}$$

where

$$F_N = \frac{F}{i_{\text{N.B.Monitor}}} \tag{32}$$

and

$$\rho_N dx_i = \frac{\int \rho dx_i}{i_{\text{N.B.Monitor}}} \tag{33}$$

The area A under the distribution curve was calculated numerically by dividing the X-axis of the curve into approximately 40 equal divisions and measuring the Y coordinate of the curve at each interval. Simpson's rule was used to calculate the integral. For the cesium and rubidium

beams, the values of A calculated in this fashion from the distribution curves were constant and reproducible within 0.5%. For potassium, the maximum variation was 1.3%.

4. Discussion of Errors

Average Velocity

Probably the largest source of error is the assumption that the velocity distribution at the neutral beam source is Maxwellian. Hundhausen and Pauly[32] reported the velocity distribution in a potassium beam effusing from an axially symmetric nozzle of 0.006" minimum diameter (compared to our rectangular nozzle of 0.004" minimum width). At a source pressure of about 5 torr (compared to 3.5 torr in our experiments) the most probable velocity was about 8% higher than that calculated assuming a Maxwellian distribution. Though a quantitative comparison is difficult, it seems reasonable to assume that the difference between the actual and calculated average velocities in our experiments may be of the same order. At any rate the ratio of mean free path to slit width (app. 0.1) certainly violates the criterion for molecular flow. We are currently planning to experimentally measure the velocity distribution from the neutral beam source under these operating conditions. Our results will be appropriately corrected.

Diatomic Molecules in the Neutral Beam

According to statistical mechanical calculations of the equilibrium constants for formation of alkali metal diatomic molecules from the atoms[33] the fractional number of diatomic molecules present in the vapor in equilibrium with the liquid at the temperatures we used is about 1%. The fraction in the beam is probably no higher than that in the source, since the contribution falls off rapidly with pressure

and only increases slightly as the temperature drops. Each of these diatomic molecules contributes two electrons to the neutral beam detector current and presumably almost nothing to the charge transfer signal, since the process is nonresonant; therefore the error in the cross section due to this factor may be about 2%. The planned experiments mentioned above will also measure the concentration of diatomics.

Ionization Coefficient

The values of the ionization coefficient used in the calculations of the cross sections are

$$\epsilon = 0.977 \text{ for cesium}$$
$$\epsilon = 0.859 \text{ for rubidium}$$
$$\epsilon = 0.690 \text{ for potassium.}$$

These were calculated from the Saha-Langmuir equation using a value of 4.58 eV for the work function of tungsten, and a temperature of 1860°K. The temperature was taken from values of the temperature versus heating current for a 0.003" diameter tungsten wire, given by Wilson and Ivanetich.[34] The ionization efficiency varies very slowly with temperature when the work function of the surface is greater than the ionization potential for the atoms. Unfortunately, slight contamination of the filament surface can have a large effect on the work function, which in turn can cause large deviations in the ionization efficiency. In particular, it has been noticed that treatment of the hot filament with hydrocarbons lowers the work function and that treatment with oxygen raises the work function. Since the detectors were always operated under conditions of $\sim 10^{-7}$ torr vacuum, and our diffusion pumps used silicone oil and were liquid nitrogen trapped,

the only contamination which is likely is due to the small amount of residual oxygen in the vacuum system. The effect of any oxygen contamination would be to increase the ionization efficiency. The error is believed to be small, but cannot be estimated quantitatively on the basis of present evidence. In any case, if the work function is higher than calculated, the maximum possible error for the cesium result at least is only 2.3%.

Contribution to the Scattering Fraction by Processes Other Than Charge Transfer

The processes to be considered are:

In the attenuation measurements

1) elastic scattering contribution

2) contribution from charge transfer ions acquiring large forward momentum in the collision

In the slow ion collection measurements

1) momentum transfer sufficient to cause the charge transfer ion to miss the detector

2) elastic scattering of primary ions into the detector

The contribution of the second process in each case is believed to be much smaller than that of the first.

It is to be expected that a part of the attenuation cross section of the ion beam is due to elastic scattering of the ions by laboratory angles greater than 25°. A crude estimation of the magnitude of the elastic contribution based on classical differential cross sections for ion-molecule scattering calculated by Mason and Vanderslice[35] gives values of a few percent of the measured cross sections.

The cross section for processes in which the ion created by charge transfer acquires sufficient momentum to avoid the detector

in the slow ion collection experiments is believed to be small based on the saturation curves for the detector current versus bias potential. In any case, the true charge transfer cross section should lie between those measured by the two methods, which in our results are equal almost to within the experimental scatter of the points.

B. Collision Cell Measurements of Product Energy and Angular Distributions from Ion-Molecule Reactions

1. General

As seen from the discussion in Chapter I, the intensity available from neutral beam sources is rather strictly limited. Even with a well designed nozzle beam source operating at high efficiency one can expect to have a particle density at the crossing point corresponding to a pressure at room temperature of only 10^{-4} torr or so. With a collision cell containing the scattering gas, however, the pressure may be increased far above this level--the only restriction being that double collisions not contribute to the measured signal. Also, the ratio of background pressure to collision cell pressure may be kept quite low by the use of small entrance and exit apertures; and the ratio of collision volume to the total ion beam volume (see Chapter I) is typically much greater than in the case of a neutral beam, resulting in a greater signal to background ratio.

The angular resolution obtained using the collision cell depends on the exit aperture and detector aperture dimensions but can easily be made equal to that obtainable when a neutral beam is used. The price one pays for the gain in product intensity by using the collision cell is a loss of resolution in the initial relative velocity of the ion and neutral.

Consider the case where a monoenergetic ion beam moving along the Z-axis of a Cartesian coordinate system intersects a collimated neutral beam moving along the X-axis. The spread in the relative speeds of ions and neutrals, under the usual condition that the ion velocity is much greater than the average neutral velocity, is due almost entirely to the spread in neutral particle velocity vector Z-components, which is zero if the beam is collimated. In the collision cell, on the other hands, the spread in relative speeds if given by the Maxwell-Boltzmann distribution of neutral particle velocities isotropically distributed around the scattering center. This spread, though generally only a small fraction of the initial ion velocity, can be important if the cross section of interest is a sufficiently rapidly varying function of velocity.

2. Experimental Arrangement and Instrumentation

The apparatus used for the collision cell experiments is shown schematically in Fig. 22. A photograph of the main chamber interior is given in Fig. 23. The electron bombardment ion source, ion focusing system, collision cell and ion counter detection system have been described previously. The only instrumentation used in these experiments and not mentioned in the discussions of the above components are a strip chart potentiometric recorder used to record the collision chamber pressure as a function of time, a Keithley Model 417 High-Speed Picoammeter used to measure the total ion beam intensity, and a Cary Model 31 vibrating reed electrometer whose input could be connected through a switch box to the detection system focusing elements (G in Fig. 15) to measure the total ion current emerging from the energy analyzer.

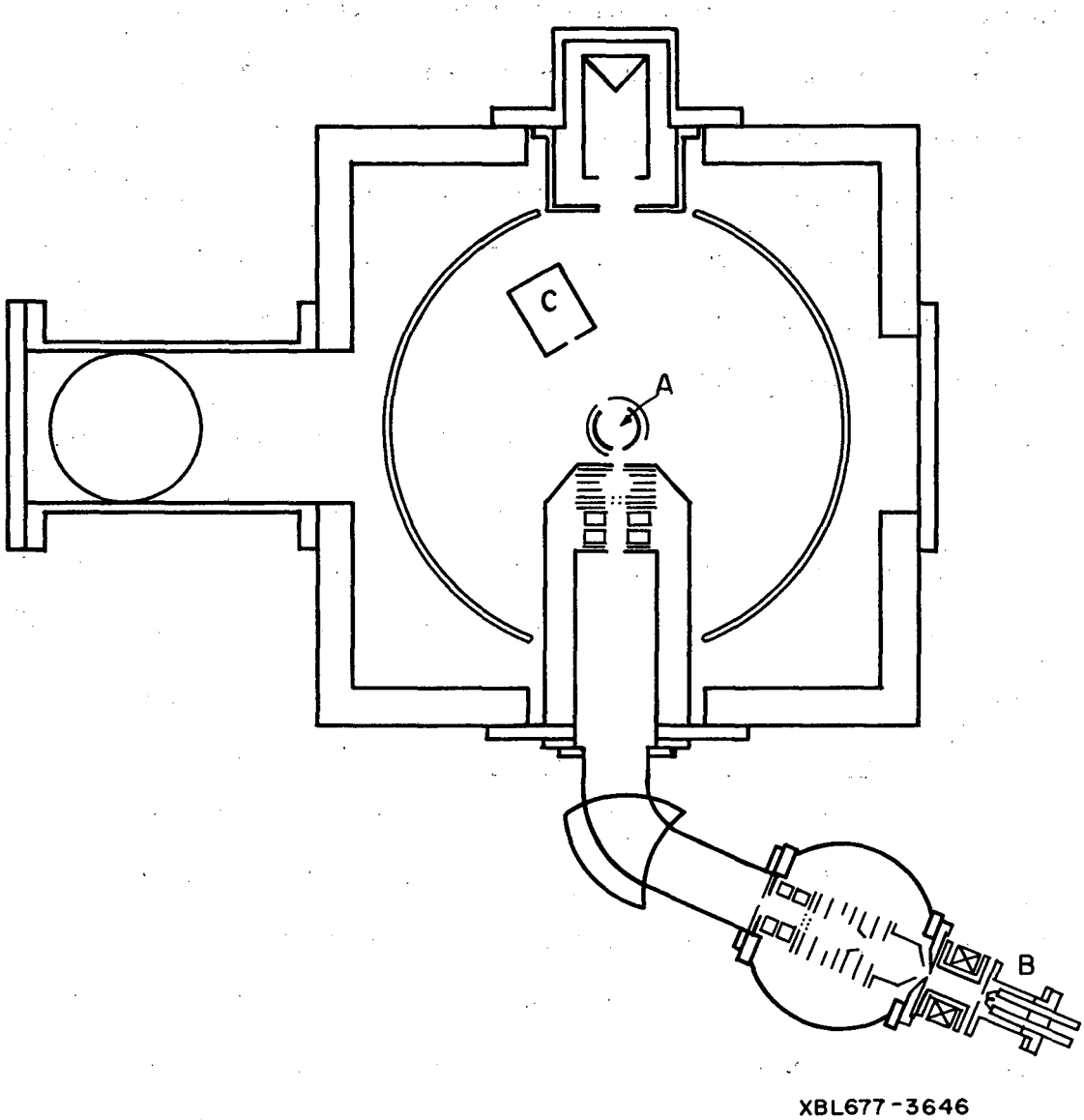

Fig. 22. Schematic diagram of the apparatus set up for collision cell measurements of product ion energy and angular distribution. The detector is shown set at $\theta = +30°$.
A Collision cell
B Ion beam source
C Detector

Fig. 23 Photograph of the main chamber interior showing ion lens focusing element shield, collision cell, and detector set at $\theta = 0°$.

A Ion beam focusing element shield

B Collision cell

C Detection system

D Copper cold shield

E Flag used to monitor total ion beam intensity

F Diffusion pump

G To diffusion pump

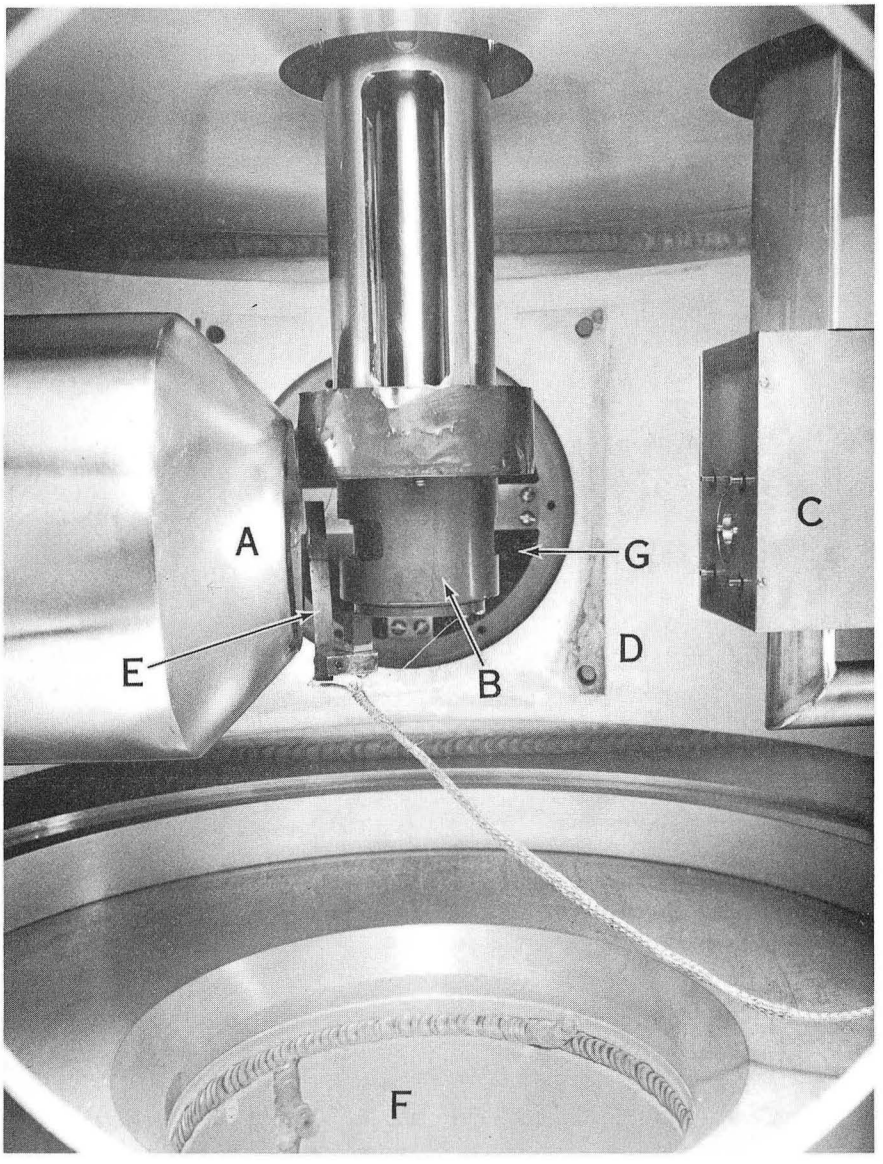

XBB 670-5730

Fig. 23.

The 78.8mm separation between the detector entrance slit of 1.5mm diameter and the 2mm diameter collision cell exit slit define a full-width geometric detector resolution of about 2.5°. Any detector angle between ±55° from the primary ion beam may be set.

3. Procedure

Relative to the involved methods used to determine the alkali metal total charge transfer cross sections, the collision cell procedure for measuring product ion energy and angular distributions is quite simple. One of the principle reasons for this is that one is usually interested in determining only relative differential cross sections, since this data can generally be normalized to known values of the absolute total cross section more accurately than the absolute values of the differential cross sections can be measured.

First an ion beam of the desired energy is produced, the analysis energy selected according to the intensity and energy resolution requirements, and the focusing adjusted to give the maximum intensity and optimum beam shape. The energy distribution of the primary beam is then determined by placing the detector in the beam and measuring with the Cary electrometer the ion current to the G focusing elements as a function of the energy analyzer potential. With the energy analyzer set to the peak energy of the beam, the angular distribution is measured by recording the electrometer current as a function of detector angle. The apparent FWHM spread of the ion beam measured in this way is typically 1.5°, which, considering the detector aperture dimension and center of rotation, actually corresponds to an almost perfectly collimated beam.

Two leak valves for the target gas are used--one which admits gas to the collision cell and the other which leaks gas directly into the main chamber for measuring the background signal due to reactions taking place outside the collision cell. The pressure of the gas in the collision cell may be monitored either with the ion gauge in the inlet tube or by means of the main chamber ion gauge, which has a reading proportional to that of the collision cell gauge. The latter method is employed when the target gas composition can be changed by reaction on the ion gauge filament. Future plans are to use a capacitance manometer to record the collision cell pressure.

To take data the detection system quadrupole mass filter is set to the appropriate mass, the angle and the energy analyzer potential set at the desired values, the detector focusing system potentials set to correspond to the energy analyzer potential (according to previously determined and tabulated values--four helipot settings are required), and the ion counting rate measured. Background signals are measured under identical conditions by cutting off the gas to the collision cell and leaking gas into the main chamber until the same background pressure is obtained. For each data point the energy analyzer potential, detector angle and collision cell pressure are recorded. At intervals of 10-30 minutes the peak primary ion beam intensity is measured as before to keep track of the drift, which is small enough to allow a linear interpolation to be used for calculating the beam intensity corresponding to each data point in the interval.

Data is generally taken in the form of constant energy or constant angle profiles of the product ion distribution. The constant energy profiles are measured by recording the counting rate at close angular

intervals with the energy analyzer and detector focusing potentials fixed. These profiles may be measured very quickly, since it takes only a few seconds to change the detector angle between measurements. The background signals are determined separately by sweeping through the angular distribution a second time. When constant angle profiles are measured, the background is determined after each data point whenever it is significant.

When it is desired to map out the entire energy and angular distribution of products at a given primary beam energy it is most convenient to take the data in the form of a series of constant energy profiles using the same detector angles and increments in each profile. The constant angle profiles may then be plotted from the same data. A typical experiment where a 25x25 matrix of intensity versus energy and angular coordinates is determined, with 20-30 seconds of counting time allotted to each point, may easily be done in an 8-hour day, including the initial ion beam and detector preparation.

4. Data Analysis

The differential cross section defined in most texts is the cross section for scattering into an element of solid angle $\sin\theta\ d\theta\ d\phi$ (in the laboratory coordinate system) or an element $\sin X\ dX\ d\phi$ (in the CM coordinate system: note that the azimuthal angle ϕ is the same in both systems). Since our experiments include velocity distribution information in addition to the angular distribution, we must redefine the differential cross section to include an element of velocity. We have some degree of choice in this matter. One possibility is to use the element $\sin\theta\ d\theta\ d\phi\ dv$, in which case one calculates the differential cross section for simultaneously scattering into the given solid angle

at a given velocity. We have chosen instead, however, to render our data in the form of the differential cross section for scattering into an element $d^3\vec{v}$ of particle velocity vector space, where

$$d^3\vec{v} = v^2 \sin\theta \, d\theta \, d\phi \, dv \, . \tag{34}$$

This choice is appealing because $d^3\vec{v}$ is the volume element in (v,θ,ϕ) space, in which the Newtonian velocity vector diagrams familiar to all molecular beam experimenters are drawn. Since the transformation from laboratory to CM coordinates in this system involves only the shift of the origin from $v = 0$ to $v = v_{CM}$, $g = 0$, where g is the velocity of the ion in the CM coordinate system, we have the simple relation

$$d^3\vec{v} = d^3\vec{g} = g^2 \sin\chi \, d\chi \, d\phi \, dg \, . \tag{35}$$

Having product ion velocity analysis, incidentally, makes the transformations between laboratory and CM coordinate systems single-valued and unambiguous, contrary to the case in which only the angular distribution information is known.

If the distribution of particle flux is defined to be $N(\theta,\phi,v)$, in units of particles/sec per unit of detection volume, then

$$dC = N(\theta,\phi,v)d^3\vec{v} \tag{36}$$

is the number of particles scattered into $d^3\vec{v}$ per second.

The differential cross section is defined as

$$I(\theta,\phi,v)d^3\vec{v} = \frac{N(\theta,\phi,v)d^3\vec{v}}{N^o\rho\ell} = \frac{dC}{N^o\,\rho\ell} \tag{37}$$

where N^o is the number of particles per second incident on the target of thickness ℓ and density ρ. In practice, however, the detector

does not subtend an infinitesimal increment of volume $d^3\vec{v}$, but a volume Z of finite size, which may be calculated by integrating $d^3\vec{v}$ over the boundaries of the detector:

$$Z = \int_{det} d^3\vec{v} = \int_{det} v^2 \sin\theta \, d\theta \, d\phi \, dv \, . \qquad (38)$$

Thus, the cross section which is measured is not the true differential cross section, which could be determined only with a detector of infinitely good resolution, but the total cross section for scattering into our detector. This cross section is

$$\int_{det} I(\theta,\phi,v) \, d^3\vec{v} = \frac{C}{N^o \rho \ell} \qquad (39)$$

where

$$C = \int_{det} dC = \int_{det} N(\theta,\phi,v) d^3\vec{v} \qquad (40)$$

is the number of particles per second striking the detector (after correction, of course, for transmission factors).

But we want to calculate a result which will converge to the true differential cross section in the limit as our detector volume Z is made smaller. This can be done by normalizing Eq. (39) to the detector volume and writing

$$\bar{I}(\theta,\phi,v) = \frac{\int_{det} I(\theta,\phi,v) d^3\vec{v}}{\int_{det} d^3\vec{v}} = \frac{C}{N^o \rho \ell Z} \, . \qquad (41)$$

Z can be calculated for our detector as follows: to first order, our detector transmits particles having energies in the band ΔE, where

$$\Delta E = kE \tag{42}$$

and k is the FWHM measure of the bandwidth. The integral over the solid angle subtended by the detector aperture is the same regardless of its orientation, and may be most conveniently evaluated at $\theta = 0$. Since the aperture is circular, the volume integral is

$$Z = \int_0^{2\pi} d\phi \int_0^{\theta^\circ} \sin\theta \, d\theta \int_{v_1}^{v_2} v^2 dv \, . \tag{43}$$

Making the reasonable approximations that $\Delta v = v_2 - v_1$ is small, and that θ°, being the small angle between a ray from the scattering center passing through the center of the detector aperture and a ray passing through the detector boundary, is equal to $\frac{1}{2}\, d/c$, where d is the aperture diameter and C its distance from the scattering center, the result is

$$Z = \frac{\pi}{4} \frac{d^2}{c^2} v^2 \Delta v \, . \tag{44}$$

Using Eq. (42) this can be rewritten in terms of the energy and product ion mass as

$$Z = \frac{\pi}{4} \left(\frac{d^2}{c^2}\right)\left(\frac{2}{M^3}\right)^{1/2} kE^{3/2} \, . \tag{45}$$

Substituting this result into Eq. (41) gives, finally,

$$\bar{I}(\theta,\phi,v) = \frac{4C}{\pi N^\circ \rho \ell} \frac{c^2}{d^2} \frac{M^{3/2}}{\sqrt{2}\, kE^{3/2}} \, . \tag{46}$$

We also note that

$$\bar{I}(\chi,\phi,g) = \bar{I}(\theta,\phi,v) \tag{47}$$

because the volume elements are equal, and because the distribution function $N(\chi,\phi,g)$ is exactly the same distribution function as $N(\theta,\phi,v)$ with its coordinate system shifted to a new origin.

For calculation of relative cross sections, the constant factors (in general: d, c, M and k) can be dropped. The data reported is actually calculated from

$$\bar{I}_{calc.} = \frac{10^7 \, S \, f(\theta)}{t \, i^{\circ} \, P \, V_{EA}^{3/2}} \tag{48}$$

where

S = number of counts recorded in time t (seconds)

P = collision cell pressure on a scale of 0 to 1000, where $1000 \cong 12\times10^{-4}$ torr

i° = peak primary ion beam current through energy analyzer in units of 10^{-12} amp

$f(\theta)$ = $\dfrac{\text{scattering volume subtended by detector at } \theta = 0^{\circ}}{\text{scattering volume subtended by detector at angle } \theta}$ (calculated graphically, assuming cutoff at slits)

V_{EA} = energy analyzer potential (volts)

The calculations are done on the CDC 6600 computer at the Lawrence Radiation Laboratory Computing Center. For each data point the product ion energy, velocity and angle in both the laboratory and CM coordinate systems and the exothermicity of the reaction at that point in $\vec{v}$ space are printed out in addition to $\bar{I}_{calc.}$. In addition, a CALCOMP plot of $\bar{I}$ vs θ or v is made of each constant energy and constant angle profile.

When a contour map of the product distribution in both velocity and angle is desired, a smoothed curve is drawn in by hand on the first set of plots, then the laboratory velocity-laboratory angle coordinates are read from the profiles at the intensities selected. These values are fed back into the computer, which transforms the coordinates to the CM system and plots the resulting coordinate pairs for each intensity on a separate graph. The final map is obtained by successively tracing the empirical contour lines on the same piece of paper.

It must be remarked in closing that $\bar{I}$ calculated as indicated above will only be a good approximation for the true differential cross section if $N(\theta,\phi,v)$ is fairly constant over the detection volume Z. Higher order corrections based on the primary beam distribution are also possible, and have recently been discussed by Ioup and Thomas.[36]

REFERENCES

1. D. R. Herschbach, Applied Optics Supplement 2: Chemical Lasers, p. 128 (1964).

2. John Ross, Ed., Advances in Chemical Physics, Vol. X, Molecular Beams (Interscience Pub. Co., New York, 1966).

3. B9, p. 250 ff.

4. B10, Ch. XIV.

5. R. L. Champion, L. D. Doverspike and T. L. Bailey, J. Chem. Phys. 45, 4377 (1966).

6. L. D. Doverspike, R. L. Champion and T. L. Bailey, J. Chem. Phys. 45, 4385 (1966).

7. Z. Herman, J. D. Kerstetter, T. L. Rose and Richard Wolfgang, J. Chem. Phys. 46, 2844 (1967).

8. B. R. Turner, M. A. Fineman and R. F. Stebbings, J. Chem. Phys. 42, 4088 (1965).

9. W. R. Gentry, Yuan-tseh Lee and B. H. Mahan, to be published.

10. W. R. Gentry, E. A. Gislason, Yuan-tseh Lee, B. H. Mahan and Chi-wing Tsao, to be presented at the Sept.1967 meeting of the Faraday Society in Toronto, Canada.

11. W. R. Gentry, E. A. Gislason, B. H. Mahan and Chi-wing Tsao, J. Chem. Phys., (in press, Sept. 15, 1967 issue).

12. D. R. Herschbach, Disc. Faraday Soc. (1962), p. 149.

13. Kent Raymond Wilson, University of California, Lawrence Radiation Laboratory Report UCRL-11605 (1964).

14. B7, p. 619.

15. B8.

16. H. U. Hostettler and R. B. Bernstein, Rev. Sci. Inst. 31, 872 (1960).

17. J. B. Anderson, R. P. Andres and J. B. Fenn, Advances in Chemical Physics, Vol. X, Ch. 8, p. 289 f (see Ref. 2).

18. C. E. Carlson and G. D. Magnuson, Rev. Sci. Inst. 33, 905 (1962).

19. K. H. Kingdon and I. Langmuir, Phys. Rev. 21, 380 (1923).

20. J. R. Werning, University of California, Lawrence Radiation Laboratory Report UCRL-8455 (1958).

21. B4, p. 382.

22. C. Lu and H. E. Carr, Rev. Sci. Inst. 33, 823 (1962).

23. E. T. S. Walton, Proc. Roy. Irish Acad. 57, 1 (1954).

24. L. A. Dietz, Rev. Sci. Inst. 36, 1763 (1965).

25. N. R. Daly, Rev. Sci. Inst. 31, 264 (1960).

26. H. M. Gibbs and E. D. Commins, Rev. Sci. Inst. 37, 1385 (1966).

27. F. S. Goulding, Nuclear Inst. and Methods 43, 1-54 (1966).

28. F. S. Goulding and D. Landis, Instrumentation Techniques in Nuclear Pulse Analysis, National Academy of Sciences--National Research Council Publication 1184.

29. Ref. 27, p.2.

30. Ref. 27, p. 26 ff.

31. Ref. 27, p. 53 f.

32. E. Hundhausen and H. Pauly, Z. f. Naturforschg. 20a, 625 (1965).

33. D. Wagman, W. Evans, R. Jacobson and T. Munson, J. Res. Nat. Bur. Standards 55, 83 (1955).

34. Kent R. Wilson and Richard J. Ivanetich, University of California, Lawrence Radiation Laboratory Report UCRL-11606.

35. E. A. Mason and J. T. Vanderslice, J. Chem. Phys. 31, 594 (1959).

36. G. E. Ioup and B. S. Thomas, J. Chem. Phys. 46, 3959 (1967).

BIBLIOGRAPHY

The following list comprises a capsule bibliography of the reviews and reference works which we found most useful in designing and constructing this apparatus.

Vacuum Techniques and Materials

B1 Fred Rosebury, Handbook of Electron Tube and Vacuum Techniques (Addison-Wesley Pub. Co., Reading, Mass., 1965).

B2 Saul Dushman, Scientific Foundations of Vacuum Technique, 2nd Ed., J. M. Lafferty, Editor, (John Wiley and Sons., Inc., New York, 1962).

B3 A. Guthrie and R. K. Wakerling, Vacuum Equipment and Techniques, (McGraw-Hill Book Company, New York, 1948).

Ion Optics and Sources

B4 Karl Ralph Spangenberg, "Vacuum Tubes", in Electrostatic Electron Optics, (McGraw-Hill Book Company, New York, 1948), Chapter 13.

B5 L. Kerwin, "Ion Optics", in Mass Spectrometry, C. A. McDowell, Editor, (McGraw-Hill Book Company, New York, 1963), Chapter 5.

B6 R. M. Elliott, "Ion Sources", in Mass Spectrometry, Chapter 4 (See B5).

B7 Manfred von Ardenne, Tabellen zur angewanten Physik, Vol. 1, Veb deutscher Verlag der Wissenschaften, Berlin (1962).

High Intensity Neutral Beam Sources and State Selection

B8 J. B. Anderson, R. P. Andres and J. B. Fenn, "High Intensity and High Energy Molecular Beams", in Advances in Atomic and Molecular Physics, Vol. 1, D. R. Bates and I. Estermann, Editors, (Academic Press, New York, 1965).

B9 H. Pauly and J. P. Toennies, "The Study of Intermolecular Potentials with Molecular Beams at Thermal Energies", in Advances in Atomic and Molecular Physics, Vol. 1, (see B8).

B10 Norman F. Ramsey, Molecular Beams (Oxford University Press, London, 1956).

APPENDIX A

List of Currently Available Mechanical Drawings

A. Molecular Beam Reaction Chamber

1.	Driven sprocket	12M7263
2.	Driven sprocket spacer	12M7273
3.	Graduated top plate	12M7284
4.	Main vacuum tank	12M5656C (MP)
5.	Side flange of top plate	12M7303
7.	Central flange of top plate	12M7312
8.	Chamber support plate	12M7334A
9.	Bearing retainer ring	12M5663A
10.	Chamber support stand	12M5796
11.	Jack screw adapter	12M5831
12.	Jack screw 3/4"	12M5841
13.	Chamber stand dolly	12M5814
14.	3/4" Jack screw bearing pad	12M5821
15.	Main tank blank flange	12M7342
16.	Top plate blank flange	12M7352
17.	Chamber window assembly	12M6294
18.	Window flange	12M6403
19.	Clamp flange	12J6771
20.	Clamp gasket	12J6781
21.	Drive sprocket	12M6302
22.	Drive sprocket support	12M7374
23.	Stop bracket	12M6411
24.	Feed thru flange	12M6422
25.	Heat shield clamp	12M6341
26.	Heat shield support bracket	12M6352
27.	Heat shield window frame	12M6364
28.	Liquid nitrogen heat shield	12M6376
29.	Liquid nitrogen supply tube	12M6396
30.	L. N. Supply tube support	12M7384
31.	Tube support bracket	12M6383
32.	Reaction chamber assembly	12M7876

B. Ion Beam Source (Alkali Metal)

1.	Mass spectrometer chamber	12M7364
2.	Test chamber vacuum seal	12M7393
3.	Magnetic analyser test chamber	12M7403
4.	Test chamber collector rail	12M7411
5.	Test chamber collector positioner	12M7421
6.	Test chamber sliding rod	12M7432
7.	Test chamber collector slit	12M7441
8.	Test chamber collector	12M7451
9.	Test chamber collector stop	12M7461

10.	Thermal ionizer chamber	12M7503
11.	Thermal ionizer unit	12M7513
12.	Thermal ionizer insulating flange	12M7522
13.	Support frame	12M7613
14.	Leveling stud	12M7624
15.	Ion beam chamber	12M7953
16.	Insulation flange	12M7963
17.	Ion beam analyzing chamber	12M7974
18.	Adaptor flange	12M7984
19.	Ion beam focusing lens	12M8131
20.	Lucite window	12M8111

C. Ion Beam Focusing System

1.	Initial focusing stage element 1	12N0332
2.	Initial focusing stage element 2, 5, and 7	12N0342
3.	Initial focusing stage element 3	12N0352
4.	Initial focusing stage element 4	12N0362
5.	Initial focusing stage element 6	12N0372
6.	Initial focusing stage element 8	12N0382
7.	Initial focusing stage element 9	12N0392
8.	Initial focusing stage element 11	12N0402
9.	Initial focusing stage quad.lens element	12N0411
10.	Initial focusing stage quad. support rod	12N0421
11.	Initial focusing stage support rod	12N0432
12.	Final focusing stage element 1	12N0442
13.	Final focusing stage element 3	12N0452
14.	Final focusing stage element 4	12N0462
15.	Final focusing stage element 5	12N0472
16.	Final focusing stage element 6	12N0482
17.	Final focusing stage element 7	12N0492
18.	Final focusing stage element 8	12N0502
19.	Final focusing stage exit slit	12N0512
20.	Final focusing stage quad. lens element	12N0521
21.	Final focusing stage support rod	12N0531
22.	Focusing element insulators	12N0542
23.	Mass spectrometer entrance slit	12N0551
24.	Mass spectrometer exit slit	12N0561
25.	Ion beam analyzing chamber modification	12N0572
26.	Initial focusing stage assembly	12N0582
27.	Final focusing stage assembly	12N0592

D. Molecular Beam Source (Alkali Metal)

1.	Liquid nitrogen cold shield	12M7472
2.	Alkali metal beam flange	12M7634
3.	Motor clamp	12M7641
4.	Beam chopper	12M7651
5.	Multichannel slit	12M7691
6.	Beam oven	12M7703
7.	Collimator slit	12M7731
8.	Beam flag	12M7661

9.	Flag stop	12M7671
10.	Flag retainer ring	12M7681
11.	Beam collimator	12M7711
12.	Knife edge slit	12M7721
13.	Slit stopper	12M7741
14.	Lamp holder	12M7751
15.	Oven set screw	12M7761
16.	Oven copper gasket	12M7771
17.	Gasket spacer	12M7781
18.	Flanged tee	12M7844
19.	Beam chamber	12M7853
20.	Blind flange	12M7862
21.	Crinkly foil spacer	12M7911
22.	Laval slit beam oven	12M8203

E. Permanent Gas Multichannel Beam Source

1.	Pump-out port	12M8281
2.	Fastener ring	12M8291
3.	Positioning screw retainer	12M8301
4.	Coupling flange	12M8313
5.	Coupling hose	12M8323
6.	Positioning screw	12M8333
7.	Mounting plate	12M8344
8.	Alignment cylinder	12M8354
9.	Gas reservoir	12M8364
10.	Assembly	12M8374

F. Supersonic Nozzle Beam

1.	Beam chamber general assembly	12M8506
2.	Collimator carriage	12M8522
3.	Position rod (1)	12M8532
4.	Position screw	12M8542
5.	Position screw retainer	12M8921
6.	Hopper gasket	12M8552
7.	Cold shield	12M8562
8.	Skimmer nozzle mount	12M8573
9.	Beam chamber shield	12M8583
10.	Chamber divider	12M8593
11.	Coupling tee and elbow	12M8604
12.	Outer coupling flange	12M8614
13.	Cold shield--liquid N_2 feed	12M8624
14.	Skimmer nozzle support	12M8634
15	Position rod (2)	12M8932
16.	Nozzle	12M8941
17.	Nozzle--gas inlet flange	12M8951
18.	Nozzle--stagnation chamber	12M8962
19.	Skimmer	12M8982
20.	Collimator	12M8972
21.	Position jack washer	12M8641
22.	Position jack	12M8652

23.	Top plate	12M8662
24.	Base plate	12M8673
25.	Supporting rack	12M8684
26.	General assembly	12M8514

G. Ion Scattering Cell

1.	General assembly	12M9073
2.	Gas inlet fitting	12M9081
3.	Pump out tube	12M9091
4.	Insulation flange	12M9101
5.	Bottom flange	12M9111
6.	Ion gauge cross	12M9122
7.	Rotation sleeve	12M9132
8.	Ion exit collar	12M9142
9.	Wilson seal mounting flange	12M9153
10.	Scattering cell	12M9163
11.	LRL standard Wilson seal (reference)	10A1111-5

H. Molecular Beam Detector (Alkali Metal)

1.	Filament support	12M7881
2.	Collector	12M7891
3.	Guard ring	12M7901
4.	Detector pillar	12M7922
5.	Detector flange	12M7933
6.	Flag shank	12M6222
7.	Flag key	12M6233
8.	Flag hoist nut	12M6241
9.	Flag nut	12M6251
10.	Flag seal nut	12M6261
11.	Detector mounting plate	12M7941
12.	Shielding can	12M8061
13.	Monitor mounting plate	12M8271

I. Molecular Beam Detector (Permanent Gas)

1.	Adjustment knob	12M8991
2.	Adjustment scale	12M9002
3.	Alignment plate	12M9012
4.	Positioning rod	12M9023
5.	Ion gauge tube	12M9034
6.	Wilson seal flange	12M9044
7.	Assembly reference	12M9054

J. Ion Beam Detector (with Retarding Electrode)

1.	Mounting plate	12M8071
2.	Shielding can	12M8081
3.	Retarding electrode holder	12M8091
4.	Ion collector	12M8101

K. Ion Detector (with QPMS and MEM)

1.	QPMS chamber	12M7806
2.	Electron multiplier chamber	12M7793
3.	Electron multiplier flange	12M7813
4.	Ion lens mounting plate	12M7821
5.	Lens electrode retainer	12M7831
6.	Ion lens mounting flange	12M8231
7.	Electron multiplier front lens	12M8241
8.	Electron multiplier middle lens	12M8251
9.	Ion extractor	12M8261
10.	4 PMS plain washer	11J8952
11.	4 PMS pigtail washer	11J8962
12.	End insulator 2	12M6003
13.	End insulator 3	12M6753
14.	QPMS pole rod	12M5982
15.	QPMS end insulator shield	12M6013

L. Ion Counter

1.	Ion counter assembly (construction detail and list of drawings and material can be obtained from this drawing)	12N0924
2.	Flat gasket 5/8 O.D.	14J9692-14
3.	Flat gasket 1 O.D.	14J9692-20
4.	Flat gasket 2-7/8 O.D.	14J9692-39
5.	Port hole cover	14J9722
6.	Feed thru mounting ring	14K1513-2
7.	Liquid nitrogen container	14K1524B-MP
8.	High voltage connector adaptor	14K3032
9.	Copper contact	14K4192
10.	Symmetrical detector heater sleeve	14K5522
11.	Symmetrical detector mount	14K5532-1
12.	Symmetrical detector mount extension	14K5542
13.	Symmetrical detector F.E.T. mount	14K5553
14.	Symmetrical detector assembly mount	14K5562-1
15.	Symmetrical detector H.V. plate	14K5572-3
16.	Symmetrical detector clamp nut	14K5582
17.	Kovar screw	12M8381
18.	Sliding seal	12M8391
19.	Ion target	12M8401
20.	Detection chamber	12M8464
21.	Cathode flange	12M8473
22.	Coupling flange	12M8483

23.	Shielding can	12M8492
24.	Shielding sleeve	12M9501
25.	High voltage protection spool	12M9512
26.	High voltage protection shield	12M9523
27.	Test shielding cup	12N0931
28.	Test flange	12N0941
29.	Support rod	12M8411

M. Fixed Faraday Cup Detector

1.	Ion collector support flange	12N0974
2.	Ion collector shield	12N0983
3.	Ion beam collector	12N0993
4.	Ion collector insulator	12N1002

N. Spherical Energy Analyzer

1.	Concave electrode	12M7091
2.	Convex electrode	12M7101
3.	Electrode mounting plate	12M7111
4.	Electrode mounting plate-2	12M7121
5.	Shielding--pumping outlet	12M7131
6.	Shielding--side plate	12M7141
7.	Slit mounting--inlet	12M7151
8.	Slit mounting--outlet	12M7161
9.	Slit base--outlet	12M7171
10.	Slit stopper--outlet	12M7181
11.	Accel-decel electrode	12M7191
12.	Metal screen mounting	12M7201
13.	Analyzer mounting plate	12M7211
14.	Analyzer mounting plate--back	12M7221
15.	Mounting frame	12M7233
16.	Shielding--slit mounting	12M7243
17.	Shielding--back	12M7253
18.	Ion lens chamber	12M7324
19.	Ion lens mounting flange	12M8151
20.	Ion lens mounting plate	12M8161
21.	Ion lens	12M8221
22.	Ion lens and plate	12M8171
23.	Blank flange	12M8211
24.	Cable positioner--1	12M7031
25.	Cable positioner--2	12M7041
26.	Electrode spacer	12M7051
27.	Electrode spacer--2	12M7061
28.	Slit insulator--outlet	12M7071
29.	Electrode holder	12M7081
30.	Cable positioner--3	12M7291

APPENDIX B

List of Electronic Prints

A. Vacuum System

1.	Standard Ion Gauge Power Supplies	5Z1814-9 LE12283-1M2
2.	Hastings single guage power supply	6Z3912
3.	Hastings dual vacuum interlock	6Z4664A
4.	Diffusion pump power interlock	8S2803
5.	Diffusion pump power interlock Model 2	8S1764

B. Experimental Instrumentation

1.	Ion source filament power supply	9S3802
2.	Spherical energy analyzer power supply	8S6121
3.	Ion detector focusing control panel	8S6131
4.	High energy ion lens voltage divider	8S4641
5.	Cold shield heater power supply	8S4371
6.	Alkali metal beam detector filament P.S.	8S4394
7.	Linear amplifier system	11X1980 P-1
8.	Print list for linear amplifier system	11X1981 P-1A
9.	FET preamplifier	11X4731 P-1
10.	Mass filter R.F. supply	8S3234-1
11.	Mass filter R.F. rectifier	8S5843
12.	Ion beam focusing control panel	8S5572

This report was prepared as an account of Government sponsored work. Neither the United States, nor the Commission, nor any person acting on behalf of the Commission:

A. Makes any warranty or representation, expressed or implied, with respect to the accuracy, completeness, or usefulness of the information contained in this report, or that the use of any information, apparatus, method, or process disclosed in this report may not infringe privately owned rights; or

B. Assumes any liabilities with respect to the use of, or for damages resulting from the use of any information, apparatus, method, or process disclosed in this report.

As used in the above, "person acting on behalf of the Commission" includes any employee or contractor of the Commission, or employee of such contractor, to the extent that such employee or contractor of the Commission, or employee of such contractor prepares, disseminates, or provides access to, any information pursuant to his employment or contract with the Commission, or his employment with such contractor.